A novel insight into the enhanced electrochemical performance of Mg-air battery in mixed aqueous and organic electrolytes

Yuxin Zhou, Xiaopeng Lu, Antoine Seyeux, Jolanta Światowska, Fuhui Wang

A novel insight into the enhanced electrochemical performance of Mg-air battery in mixed aqueous and organic electrolytes

Yuxin Zhou[12], Xiaopeng Lu[1*], Antoine Seyeux[2], Jolanta Światowska[2*] and Fuhui Wang[1]

[1]Corrosion and Protection Center, Northeastern University, Shenyang, 110819, P. R. China

[2]Chimie ParisTech - CNRS, PSL University, Institut de Recherche de Chimie Paris, 11 rue Pierre et Marie Curie, Paris 75005, France

**Corresponding author: Dr. Xiaopeng Lu (luxiaopeng@mail.neu.edu.cn) and Dr. Jolanta Światowska (jolanta.swiatowska@chimieparistech.psl.eu)*

Abstract

A new strategy of utilizing mixtures of ethanol and complexing agents on Mg-air battery is investigated systematically. The presence of ethanol promotes formation of a dense inner layer with a high portion of oxide in the discharge film, leading to significantly enhanced utilization efficiency. The highest utilization efficiency of Mg anode has been increased from 53.6 % to 85.7 % and the discharge potential is decreased 300 mV, when discharges in mixed electrolyte. The adsorption/deposition of S-like species on metal surface is evidenced in ethanol and 5-sulfosalicylate acid containing solution, resulting in inhibition of the hydroxide-rich outer layer growth.

Keywords: Primary Mg-air battery; Utilization efficiency; Time-of-flight secondary ion mass spectrometry; Additive

1. Introduction

The high volumetric capacity (3832 mAh g^{-1}) and low standard electrolyte potential (-2.37 V vs. SHE) of Mg make primary Mg-air batteries a promising power source for offshore devices and electric vehicles [1-6]. However, practical application of Mg-air battery is greatly limited due to two main issues [7-13]. Firstly, rapid self-corrosion rate of anode, related to high hydrogen evolution rate (HER) during discharge, which largely reduces the utilization efficiency of the Mg anode and shortens its service life. Secondly, appearances of undissolved discharge products on anode surface, which induces significant decrease of reaction kinetics, and is detrimental to the discharge

voltage. In this case, undissolved Mg matrix appears on discharge products and dissolve into electrolyte, further reducing the utilization efficiency and specific capacity of anode [14, 15]. It has been proved that tailoring the chemical composition of the anode or electrolyte can effectively enhance the discharge performance of Mg-air batteries.

Alloying or heat treatment of Mg-based electrode materials is beneficial to change the phases (composition or morphology) inside, which leads to uniform dissolution during battery operating and high discharge performance [4, 16-23]. Deng et al. [18] found that the redeposition of In element at the interface of substrate/oxide film disrupted the discharge product film and inhibited the NDE effect of the anode. Mg-0.1Ca-0.2In alloy exhibited superior utilization efficiency, e.g., 80.2% at 5 mA cm^{-2}. It was reported by Sha et al. [19] that addition of 0.5 wt.% Y element promoted the formation of intermetallic phase ($Mg_{24}Y_5$) in Mg-4Li anode. The $Mg_{24}Y_5$ phase facilitated the grain refinement of Mg-4Li alloy, which reduced the weight loss during discharge. Chen et al. [4] concluded that heat treatment greatly reduced the potential difference between Mg matrix and second phases (Mg_7Zn_3 and $Mg_{17}Al_{12}$). The micro-galvanic corrosion process of Mg alloys was inhibited and high utilization efficiency of Mg-6Zn alloy was enhanced from 44% to 56% after heating at 693K for 20 h.

The modification of electrolyte through the addition of specific compounds has a significant effect on improving the discharge performance of Mg-air batteries [5, 14, 24-34]. It has been reported that complexing agents can act as electrolyte additives due to their Mg^{2+} and Fe^{3+} complexing ability [25, 26, 35, 36]. The strong Mg^{2+}complexing agent effectively removes discharge products and maintains a stable discharge voltage. Furthermore, the addition of complexing agents chelates with Fe^{3+} and inhibits the micro-galvanic corrosion process, leading to increased utilization efficiency. It was verified by Vaghefinazari et al. [31] that ethylendiaminetetraacetic acid (EDTA) prevented the deposition of discharge products and decreased the self-corrosion process caused by the re-deposition of Fe. The electrochemical activity of anode was greatly enhanced and 1.62 V of discharge voltage was shown after introduction of 0.1 M EDTA at 5 mA cm^{-2}. Wang et al. [28] investigated that the effect of different concentrations of 2,6-dihydroxybenzoate (2,6-DHB) on the discharge performance of the Mg anode. It

was demonstrated that 0.2 M 2,6-DHB was sufficient to hinder the deposition of discharge products on surface. The HER of anode during discharge was inhibited in 0.2 M 2,6-DHB containing solution and the specific energy of AM50 Mg alloy was increased from 1640 to 1850 Wh kg^{-1} after the introduction of 0.2 M DHB at 10 mA cm^{-2}. Complexing agents accelerate the dissolution rate and enhance the transfer process of ions. However, Mg anode shows high self-corrosion rate during discharge with addition of strong Mg^{2+} complexing agent, which decreases the utilization efficiency and specific capacity, especially under low current densities.

Recently, it was found that organic solvent has a great effect on regulating the electrochemical behavior of the Mg anode [11, 37, 38]. Kurchavov et al. [38] investigated the NDE of Mg sample in ionic liquid and water mixture electrolytes, more specifically in $[mPEG_nMPyr]AcO\text{-}H_2O$. They concluded that oxygen atoms of $[mPEG_nMPyr]^+$ bonded the released water, leading to the great inhibition of the reaction between free H^+ and Mg sample. The mixture of water/organic electrolytes can also be efficient to decrease the corrosion of Mg-based anode. It was demonstrated that 0.5 wt.% ethanol enhanced the corrosion resistance of Mg sample and reduced the actual weight loss during discharge [37]. The composition of discharge products showed a decreased of $Mg(OH)_2$ deposition on surface, which enhanced the discharge performance of anode. Nevertheless, the improvement of utilization efficiency and specific capacity by ethanol was shown to be limited and the Mg anode demonstrated low discharge voltage compared to that in blank NaCl solution.

Strong Mg^{2+} complexing agents (Mg^{2+} constant stability > 5) might have great potential to increase the electrochemical activity of anode [8, 35, 39]. Therefore, three complexing agents are selected as electrolyte additives in the present study: 4,5-dihydroxy-1,3-benzenedisulfonic acid disodium salt (Tiron), 3,4-dihydroxybenzoic acid (3,4-DHB) and 5-sulfosalicylic acid (SSA). The Mg^{2+} constant stabilities of the complexing agents are listed in Table S1. In order to inhibit the detrimental effect of H^+ on the self-corrosion process of Mg sample, ethanol is used as another additive into electrolyte. In present experiment, the impact of additives on the discharge performance and corrosion of pure Mg in NaCl solution, their effect on the discharge products and corrosion

mechanism are investigated. Specifically, the composition and distribution of discharge products on surface in different solutions is investigated. Moreover, the discharge mechanism through the electrolyte additives that enhanced the discharge performance of anode is also clarified.

2. Experimental methods

2.1. Preparation of anodes and electrolytes

In this study, commercial pure Mg samples, the same as in our previous studies [40], were used as the anodes. All specimen were ground by using silicon carbide papers and dried in air (2000 grit). The based solution used in this study was 3.5 wt.% NaCl electrolyte, and the additives included 30% volume of ethanol (> 99.9%), 0.1 M 4,5-dihydroxy-1,3-benzenedisulfonic acid disodium salt (Tiron), 0.1 M 3,4-dihydroxybenzoic acid (3,4-DHB) and 0.1 M 5-sulfosalicylic acid (SSA) (MacLin, Shanghai, China). The pH of different electrolytes was tailored to a pH of 7 ± 0.2 by using NaOH. The conductivity and resistivity of various solutions were measured by ROOKO Surface Resistance Tester (FT-400AHXM, Ningbo, China) according to MIL-DTL-81706B.

2.2. Electrochemical tests of samples

A comprehensive description of experimental details is provided in supplementary material.

2.3. Analysis of sample and electrolyte after discharge

After discharge, the morphology of Mg sample was detected by scanning electron microscope (Quanta250FEG, FEI, USA). X-ray diffraction (XRD) equipped with Cu K α radiation was carried out using a Smartlab instrument (Model SmartLab, Rigaku, Tokyo, Japan) to analysis the discharge products formed on surface. The step size for the XRD test was 5° min^{-1} and the test was conducted in the range of 10° to 90°. Raman spectra was collected in the range of 4000–50 cm^{-1} on Raman microscope (Model RXploRA Plus, Horiba, Kyoto, Japan) to confirm the composition of discharge products after discharge in mixtures. Hydra/Medusa® software (USA) was carried out to simulate the chemical composition of surface and electrolytes after discharge for 10 h.

Time-of-flight secondary ion mass spectrometry (ToF-SIMS) was utilized to investigate the composition and distribution of species on anode surface after discharge for 5 min in different solutions. A ToF-SIMS V spectrometer (ION TOF Münster, Germany) with an operating pressure of 10^{-9} mbar was employed for ToF-SIMS in-depth profiling. For further analysis, a pulsed 25 keV Bi^+ primary ion source delivering a 1.2 pA current over a 100 × 100 μm^2 area was performed. Sputtering was adopted by 2 keV Cs^+ giving a 100 nA target current over 300 × 300 μm^2 area. The analysis was performed in the negative mode to get better sensitivity to the oxide species. Flood-gun was employed for charge neutralization. Analysis of post-processing and data acquisition was used with the Ion-Spec software (version 4.1).

3. Results

3.1. Electrochemical measurements

3.1.1. EIS test

Fig. 1 displays the impedance spectra of the Mg sample after being immersed in various electrolytes for 1 h. The spectra was fitted using the equivalent circuit depicted in Fig. 2a, where R_s corresponds to the solution resistance, R_f and CPE_f represent the resistance and capacitance of corrosion product film, respectively, R_{ct} represents the resistance of charge transfer, while CPE_{dl} stands for the capacitance of double layer [41, 42]. The inductive loop observed at low frequency is influenced by the possible non-stationary state, which is discarded from the fitting process [43]. The fitted EIS results are displayed in Fig. 2b and Table 1.

The largest capacitive loop can be observed with the addition of ethanol (Fig. 1a). As shown in Fig. 1b, the impedance value at low frequency rises from 523 $\Omega \cdot cm^2$ (for NaCl) to 5720 $\Omega \cdot cm^2$ (for ethanol), suggesting that the degradation behavior of Mg is inhibited in ethanol containing electrolyte. The inhibition is also confirmed from a significant increase of the R_{total} (sum of R_f and R_{ct}) by 4890 $\Omega \cdot cm^2$ with reference to the NaCl electrolyte (Fig. 2b and Table 1).

However, the dissolution process of Mg samples is significantly promoted by the presence of Mg^{2+} complexing agent in solutions without ethanol. A narrow capacitive loop and a visible inductive loop can be observed in the presence of Tiron for 1 h (a

zoom of Nyquist plot presented as an inset in Fig. 1a). In this solution, the lowest impedance value at 0.01 Hz reduced by 513 $\Omega \cdot cm^2$ is observed with reference to the NaCl electrolyte (Fig. 1b). Similarly, significant dissolution of the Mg sample can be also confirmed in 3,4-DHB containing solution as the low impedance (Fig. 1b) and a narrow phase angle (Fig. 1c). Slightly higher impedance as well as larger phase angle can be detected for SSA complexing agent. However, it can be found that introduction of complexing agent contributes to high dissolution rate of Mg sample, as evidenced by the small capacitive loop, low impedance and small phase angle (Fig. 1a, b and c, respectively). It is also observed from Fig. 2b and Table 1 that the R_{total} decreases to 6.8, 19.8 and 160.6 $\Omega \cdot cm^2$, respectively in Tiron, 3,4-DHB and SSA containing solution, further indicating the high dissolution rate of Mg samples in these solutions.

In mixtures, when the ethanol is added to the electrolytes containing the complexing agents, the increase of impedance value at low frequency (Fig. 1b) and the wider phase angle (Fig. 1c) are regularly observed. The highest increase can be noticed in 3,4-DHB and ethanol solution, where the impedance value at low frequency reaches 112.5 $\Omega \cdot cm$, which indicates 5-fold increase with reference to a single 3,4-DHB solution (Fig. 1b). This indicates that the dissolution rate is reduced in the mixture solutions compared to the single complexing agent solutions based on water solvent. Comparing to value of R_{total} after fitted, it could be verified that Mg samples show higher corrosion resistance in mixtures than in solutions with addition of single complexing agents (Fig. 2b and Table 1). For instance, the R_{total} of Mg sample increases to 109.8 $\Omega \cdot cm^2$ after immersion in 3,4-DHB and ethanol containing solution. Mg sample shows 160.6 $\Omega \cdot cm^2$ of R_{total} after soaking in the presence of SSA and ethanol, which is 311.5 $\Omega \cdot cm^2$ higher than in the water-based solution.

The compactness and thickness of corrosion film can be also evaluated by impedance spectra (Fig. 2 and Table 1). Due to the porosity, roughness, and non-uniform conductivity of surface layer, a non-ideal capacitive behavior (CPE) was used to fit the double-layer capacitor, which deviate from ideal dielectric behavior [44, 45].

To account for the corrosion film formed on the surface in different solutions, two parallel capacitances are used. The final capacitance value (CPE) can be determined using equation (5) [44]:

$$CPE = S\ CPE_{dl} + (1 - S)\ CPE_f \quad (5)$$

S represents the fraction of the active surface, corresponding to substrate exposed to electrolyte (which can be found in the film pores and defects). Depending on the property of corrosion film formed on surface, CPE_f is used for evaluating the CPE of film in electrolyte with single ethanol (protective film) whereas CPE_{dl} plays a dominant role in determining CPE of films in other electrolytes (defective films, as evidence by the narrow capacitive loops and phase angles) [37, 46]. Table 1 also shows the CPE_{dl} of 10^{-2} and n_{ct} value of 0.99 (close to 1) in electrolyte with addition of single Tiron. This implies that the CPE corresponds almost to a double layer capacitance of 10^{-2} F cm^{-2} in this solution [47].

The effective capacitance (C_{eff}) was calculated using the simplified Brug formula (6), where R_s can be ignored when R_s is much smaller than R_{ct} and R_f [46, 48]:

$$C_{eff} = CPE^{\frac{1}{n}} (R_s)^{\frac{1-n}{n}} \quad (6)$$

It is found that C_{eff} value for the single ethanol containing solution (1.3×10^{-5}) is the lowest among various solutions (Table 1).

The thickness of the surface film can be calculated using the Cole-Cole diagram [49, 50]. To do so, the complex capacitance C(ω), expressed by equation (7), needs to be determined [49, 51]:

$$C(\omega) = \frac{1}{j\omega(Z(\omega) - R_e))} \quad (7)$$

Where ω is equal to 2 × Π × f (frequency) Hz, Z(ω) is related to impedance value, and R_e represents the solution resistance from fitting process.

From equation (7), the real and imaginary parts of C(ω) can be separated, resulting inand two equations, (8) and (9) [49]:

$$Re\big(C(\omega)\big) = -\frac{Im(Z)}{\omega(Re(Z)^2_{corr} + Im(Z)^2)} \quad (8)$$

$$Im(C(\omega)) = -\frac{Re(Z)_{corr}}{\omega(Re(Z)^2_{corr}+Im(Z)^2)} \quad (9)$$

The limit of Re(C(ω)) at infinite frequency is the infinite capacitance C(∞), which is used for calculating the thickness of film using equation (10) [49, 51]. In the case of current work, C(∞) is determined at frequency of 10 kHz.

$$\delta = \frac{\varepsilon\varepsilon_0}{C_\infty} \quad (10)$$

In this equation, ε is the relative dielectric constant of MgO (ε =10), and ε_0 is the vacuum permittivity ($\varepsilon_0 = 8.85\times10^{-14}$ F cm^{-2}) [52]. The calculations reveal that a 194 nm-thick corrosion film is formed in blank NaCl solution, while significantly smaller values were observed in solutions containing single complexing agents. For example, a 54 nm-thick film was formed on the surface in the presence of Tiron (Table 1). The highest film thickness observed in blank NaCl solution implies that significant amounts of corrosion products accumulate on the surface, due to severe corrosion occurring during the immersion process. The presence of single ethanol is effective in slight reducing the film thickness, as evidenced by the formation of a 185 nm-thick surface layer (Table 1), indicating the lower corrosion rates. Thicker corrosion films are formed on the surface with addition of the mixtures compared to those containing single complexing agents. For instance, the film thickness is 159 nm in solution with Tiron and ethanol, which is 105 nm thicker with reference to the single Tiron containing solution (Table 1). The modifications and the properties of the surface layers across different electrolytes will be addressed in the discussion section. It is important to note that for this calculation is assumed that the film is only composed of MgO and the dielectric constant of MgO is used for calculation. The actual corrosion film contains high amounts of $Mg(OH)_2$, thus estimating the total film thickness by only considering MgO might be inaccurate.

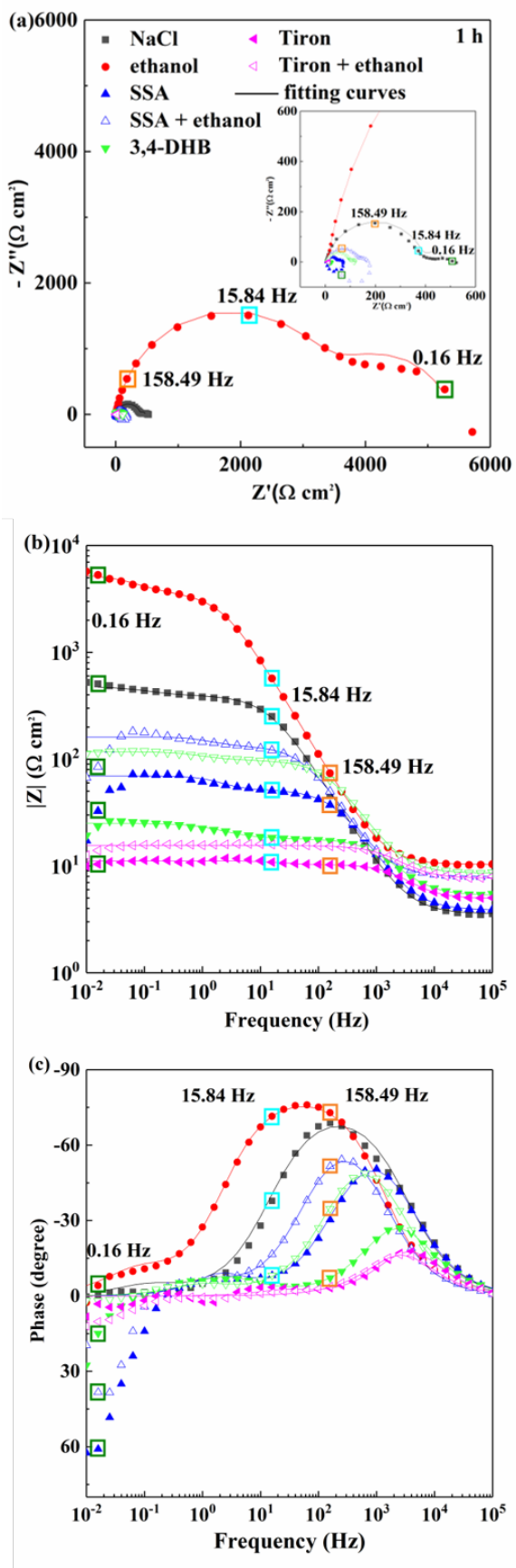

Fig. 1. EIS spectra of Mg samples after 1h-immersion in various electrolytes: (a) Nyquist plot, (b) Bode plots impedance spectra and (c) Phase angle.

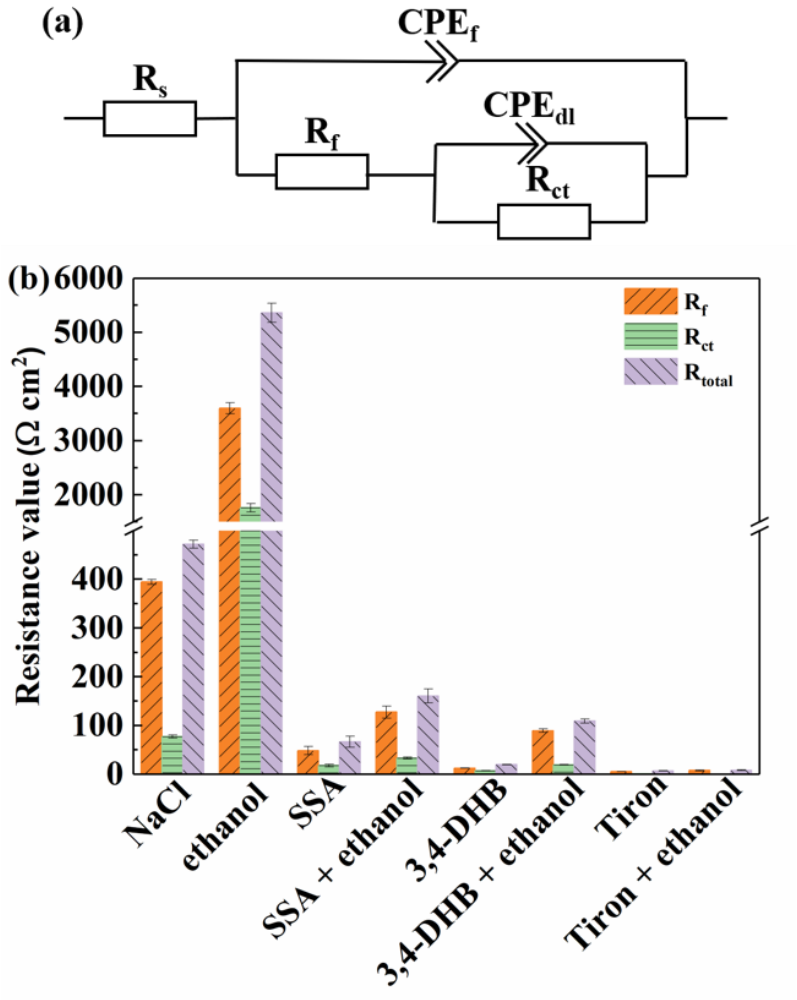

Fig. 2. Equivalent circuit used for the EIS fitting (a) and values of resistances (b) for Mg specimen after 1h-immersion in different electrolytes.

Table 1. Fitting values obtained for components of EIS equivalent circuit for Mg sample after immersion in various electrolytes with additives for 1 h.

Electrolyte	R_s (Ω cm^2)	CPE_f ($\Omega^{-1}s^{-n}$ cm^{-2})	R_f (Ω cm^2)	n_f	CPE_{dl} ($\Omega^{-1}s^{-n}$ cm^{-2})	R_{ct} (Ω cm^2)	n_{ct}	R_{total} (Ω cm^2)	C_{eff} (F cm^{-2})	d (nm)
NaCl	3.5±0.1	5.2×10^{-5}	394.6±5.2	0.98	9.1×10^{-5}	77.5±3.1	0.99	472.1±8.3	1×10^{-4}	194
NaCl + ethanol	10.3±0.2	2.9×10^{-5}	3600±101	0.91	5.3×10^{-3}	1762±76	0.88	5362±177	1.3×10^{-5}	185
NaCl + SSA	3.3±0.3	3.0×10^{-5}	48.6±8.3	0.88	4.0×10^{-3}	17.9±2.9	0.95	66.5±11.2	5.6×10^{-3}	86
Mix NaCl + SSA + ethanol	7.9±0.1	4.4×10^{-5}	127.4±12.4	0.88	7.2×10^{-3}	33.2±1.6	0.92	160.6±14	1.3×10^{-2}	168
NaCl + 3,4-DHB	3.3±0.1	3.6×10^{-5}	12.7±0.2	0.87	1.7×10^{-2}	7.1±0.2	0.85	19.8±0.4	3.9×10^{-2}	66
Mix NaCl +3,4-DHB + ethanol	8.5±0.3	2.7×10^{-5}	89.5±3.5	0.88	1.1×10^{-2}	19.6±0.6	0.89	109.1±4.1	2.4×10^{-2}	165
NaCl + Tiron	3.4±0.2	3.3×10^{-5}	5.5±0.2	0.89	1.0×10^{-2}	1.3±0.1	0.99	6.8±0.3	1.1×10^{-2}	54
Mix NaCl + Tiron + ethanol	7.7±0.1	3.4×10^{-5}	7.8±0.8	0.88	6.6×10^{-3}	0.4±0.2	0.99	8.2±1	7.1×10^{-3}	159

3.1.2. Polarization test

The corrosion behavior of Mg specimen after soaking in various solutions for 1 h is evaluated by polarization test, as shown in Fig. 3. Table S2 lists the corrosion potential (E_{corr}) and corrosion current densities (i_{corr}) of the samples.

The lower anodic and cathodic current densities are observed for Mg sample in NaCl solution with ethanol, indicating that ethanol inhibits the anodic dissolution process and cathodic H_2 evolution reaction. The corrosion density of Mg specimen decreases by 120 μA cm^{-2} due to the introduction of ethanol (Table S2), which confirms the improved corrosion resistance.

However, after addition of complexing agents to the NaCl electrolyte, i_{corr} of Mg sample significantly increases. For instance, the i_{corr} of sample reaches 13943.4 μA cm^{-2} in the presence of Tiron. This reflects that Mg sample shows high dissolution rate in the presence of single complexing agent. It should be noted that the anodic branches move towards higher current densities, confirming the promotion of dissolution process.

In comparison to blank NaCl solution, the anodic and cathodic branches shift to the higher currents in the presence of mixtures. It means that Mg samples show higher dissolution rates in mixtures (complexing agents and ethanol) than in the water-based solutions. However, after exposition to the mixtures for 1 h, lower i_{corr} of Mg sample can be observed (7348.3 μA cm^{-2}) in Tiron and ethanol containing solution than a single Tiron (13943.4 μA cm^{-2}). In the case of 3,4-DHB and ethanol mixture, the i_{corr} is ten times lower than in the case of simple addition of complexing agent (764.1 vs 7235.5 μA cm^{-2}, respectively). Thus, single ethanol is efficient in decreasing the corrosion rate of Mg in comparison to the solution with a single complexing agent.

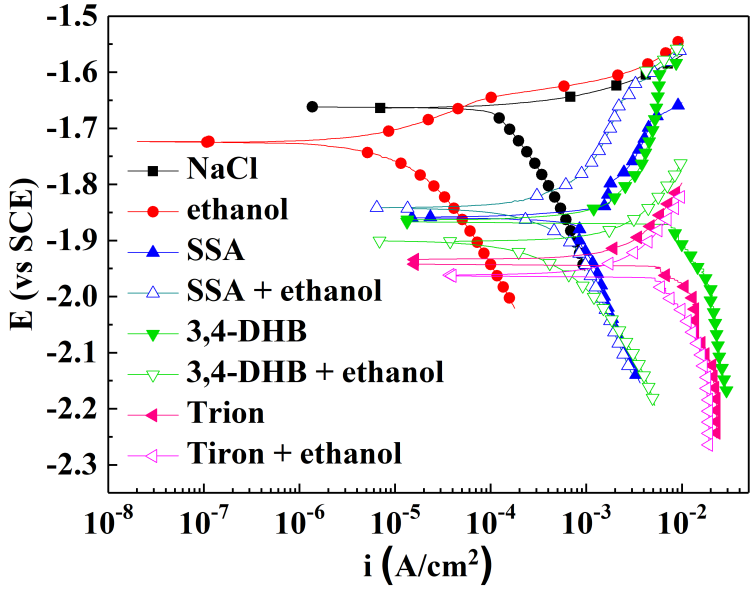

Fig. 3. Potentiodynamic polarization curves of Mg specimen after 1h-immersion in various electrolytes.

3.2. Discharge properties of anode in half-cell test

The discharge property of Mg samples exposed to NaCl solutions with and without additives is investigated using half-cell discharge test.

Similar OCP in ethanol containing solution with reference to based solution can be observed, which implies that single ethanol has a week effect on enhancing the electrochemical activity of Mg sample (Fig. 4a and Table 2).

The Mg anode demonstrates low open circuit potential (OCP) in the presence of single complexing agents. The lowest OCP of -1.94 V is observed in the presence of Tiron. After addition of SSA and 3,4-DHB, the OCP of Mg anode decreases to -1.86 V (Fig. 4b and Table 2). The relatively low OCP of the Mg anode indicates high electrochemical activity of Mg sample in these solutions. Complexing agents effectively decrease the discharge potential of the anode at different current densities (Fig. 4b-d and Table 2). At 2.5 mA cm^{-2}, a discharge potential of -1.92 V is observed after introduction of Tiron and -1.83 V in the presence of 3,4-DHB. As for SSA, the average potential of specimen significantly decreases from -1.62 to -1.8 V (Fig. 4). As the current density increases, Mg samples still show high dissolution behavior in NaCl

solution with single complexing agents (Table 2 and Fig. 4d). Apparently, discharge potential of -1.79 V is demonstrated for Mg in single Tiron containing solution. With the addition of 3,4-DHB, the discharge potential of the Mg anode is still 40 mV lower than that of blank NaCl solution.

In mixture solutions, OCP of Mg sample decreases with the lowest value of -1.96 in Tiron and ethanol. Other mixtures also have great influence on decreasing the OCP of Mg sample (Fig. 4a and Table 2). Interestingly, the effect of mixtures on the discharge behavior changes with the increase of current density. At 2.5 mA cm^{-2}, it is worth noting the lower discharge potential with addition of ethanol and Tiron (-1.9 V) compared to that in NaCl solution (-1.62 V). At the same current density, in the presence of ethanol and SSA, the Mg anode shows a discharge potential of -1.68 V, which is 60 mV lower than that of the reference (Fig. 4b).

Discharge potential of samples increases as current density increases (Fig. 4c and d) in mixtures. It is illustrated that Mg sample exhibits a high discharge potential of -1.61 V with the addition of SSA and ethanol. A similar average anode discharge potential is observed after introduction of 3,4-DHB and ethanol. When a current density of 10 mA cm^{-2} is applied, the discharge potential of the Mg anode sharply increases after discharging for 5 h in mixtures containing SSA and 3,4-DHB (Fig. 4d).

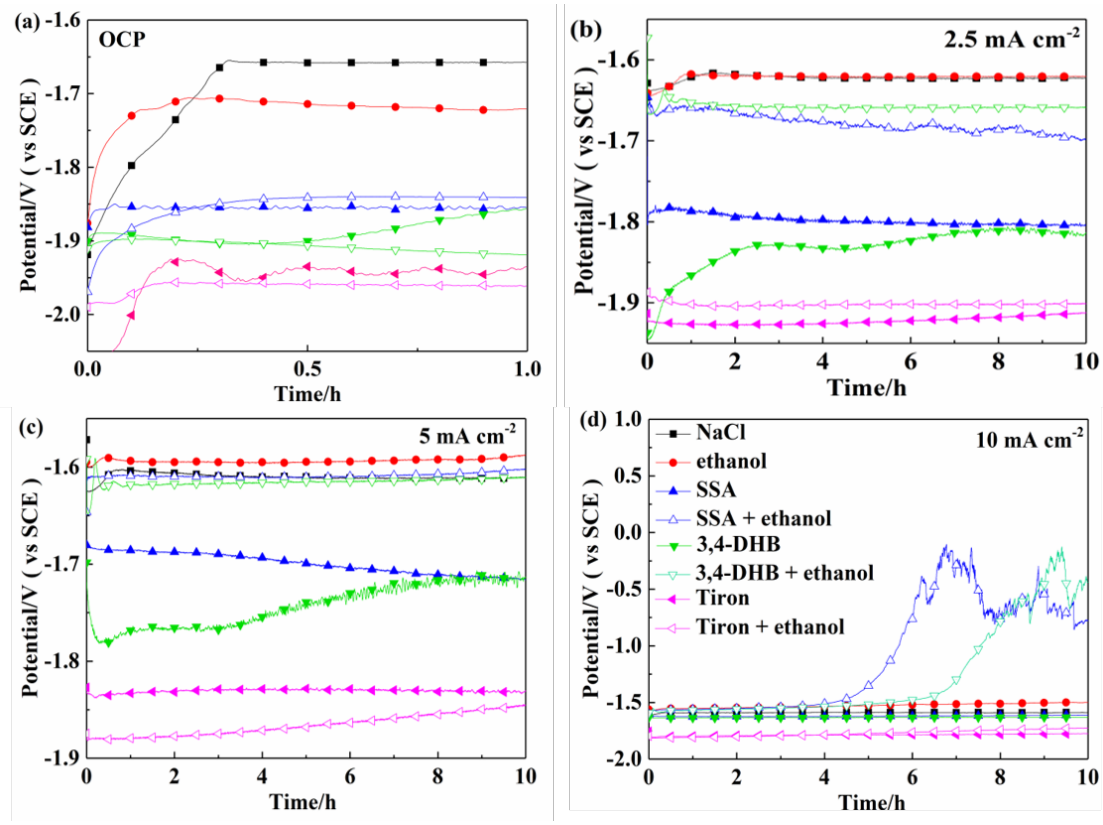

Fig. 4. Electrochemical behaviour of samples in NaCl electrolytes with or without additives. (a) OCP, (b) 2.5 mA cm^{-2}, (c) 5 mA cm^{-2} and (d) 10 mA cm^{-2}.

This significant rise in discharge potential may be attributed to the high solution resistance and the substantial deposition of discharge products. Equation 5 is employed in order to explain the discharge potential of anode in solutions with or without additives at different current densities [39, 53].

$$E_{anode} = E_{ocp} - \eta_{ct} - \eta_{diff} - IR \quad (11)$$

The average open circuit and discharge potential is presented by E_{ocp} and E_{anode}, respectively, η_{ct} corresponds to the drop of potential induced by resistance of charge transfer, η_{diff} to the overpotential of diffusion resulted from the discharge product, and IR to the potential drop, which is related to the applied current density and solution resistance. Except from solution with single ethanol, low OCP of anode is demonstrated after introduction of different additives. However, Mg samples show higher discharge potentials in ethanol and mixture solutions than in blank water-based solution at high current densities. It means that the η_{ct}, η_{diff} and IR determine the average discharge potential of Mg sample. Table S3 displays the conductivity and resistivity of different electrolytes that are used in this study. It can be seen that

introduction of ethanol increases the resistivity of electrolyte due the reduction of free H^+. High current density further leads to the large potential drop. Similarly, the potential drop (IR) is larger in mixtures than in NaCl-based solutions, especially at high current densities (Table S3). On the contrary, single complexing agents leads to the increase of the conductivity of solution due to the dissociation of molecules (Table S3). Thus, the IR after addition of single complexing agents is lower than that of NaCl solution.

Fig. S1 shows the EIS spectrum of discharged samples in various electrolytes. The wide capacitive loops can be observed for all current densities in electrolytes containing ethanol (Fig. S1a-c), indicating the large η_{ct} and η_{diff} during discharge. However, Mg samples show narrow capacitive loops in solutions with single complexing agents (Fig. S1a-c), implying that single complexing agents have great effect on reducing the η_{ct} and η_{diff}. Apparently, the narrowest capacitive loop is shown in the presence of 0.1 M Tiron containing solution. In case of mixture solutions, Mg samples show narrow capacitive loops after discharge (Fig. S1a), especially in solution composed of Tiron and ethanol. However, as the applied current density increases, the capacitive loops in mixtures (SSA and ethanol, 3,4-DHB and ethanol) become more wider compared to those in NaCl solution. This widening suggests increased charge transfer and diffusion resistance (η_{ct} and η_{diff}) at high current densities (Fig. S1b and c).

Fig. 5 displays the optical morphology of discharged samples in different electrolytes. The apparent discharge products deposits on anode surface in NaCl solution and ethanol containing solution (Fig. 5a, b, e and f) could be observed. However, the presence of discharge products is scarce in solutions containing complexing agents (Fig. 5d, h, j, n, l and p). This confirms that the contributions of η_{ct} and η_{diff} resulting from discharge products in solutions with single complexing agents are minimal. In the case of mixture solutions, a smaller accumulation of discharge products appears on surface in solutions containing Tiron and ethanol (Fig. 5i and m). Mixtures containing 3,4-DHB and ethanol, SSA and ethanol effectively suppress the appearances of discharge products (Fig. 5c and k). However, with the increase of current density, significant amounts of discharge products accumulate on surface in these two mixtures (Fig. 5g and o), which is detrimental to the discharge process of the Mg anode. The surface state of discharged specimen, as observed through optical microscopy, correlates with the impendence test.

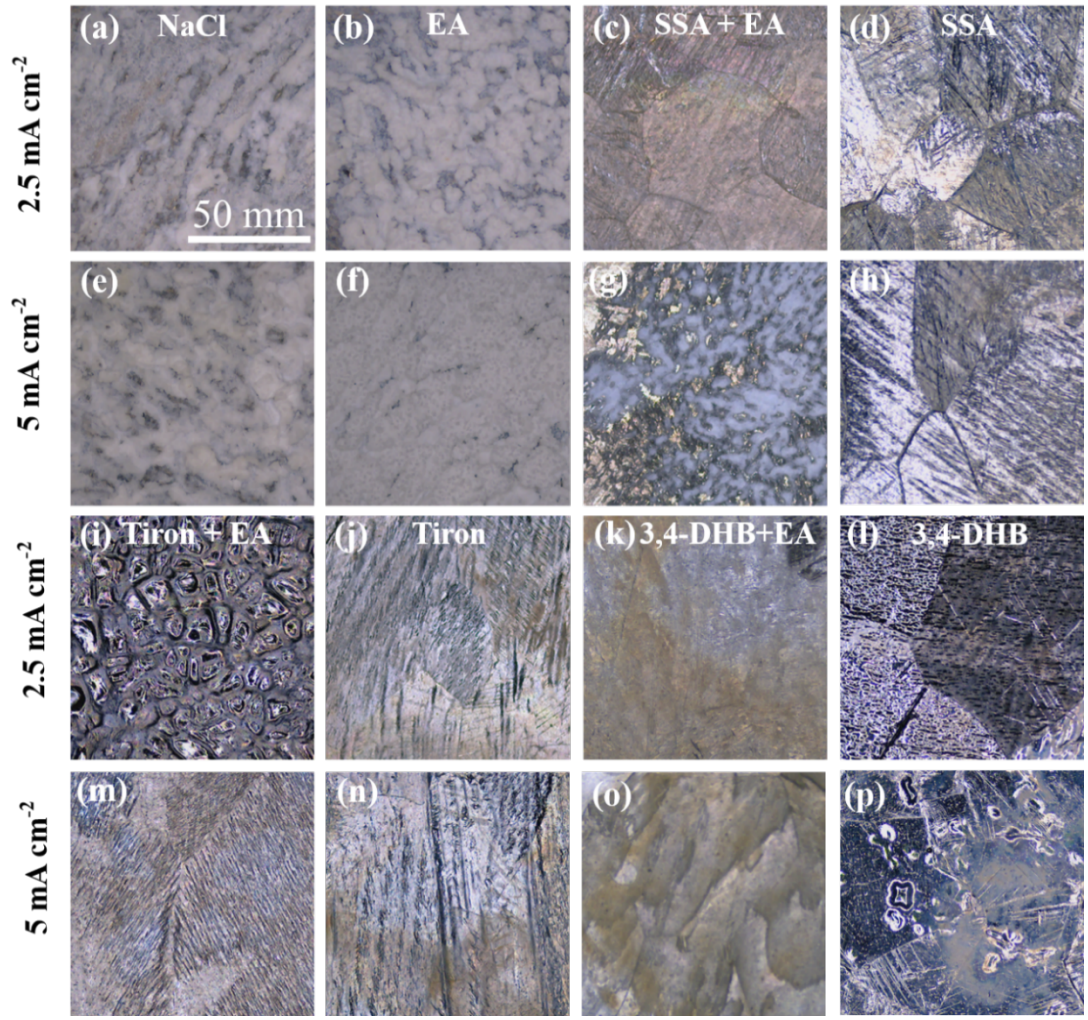

Fig. 5. Optical surface micrography of Mg samples after discharge at different current densities for 10 h in various electrolytes.

In order to investigate the reason of the sharp increase in discharge potential observed in mixtures during discharge at 10 mA cm^{-2}, the composition of discharge products is examined using X-ray diffraction (XRD) and Raman spectroscopy (Fig. 6). It is evident that discharge products, primarily consisting of $Mg(OH)_2$, deposit on the surface after discharge in various solutions for 10 hours. The substantial accumulation of discharge products impedes the contact area between the anode and the electrolytes, thereby contributing to the high discharge potential (Fig. 6a). As shown in Fig. 6b, peak at 3474 cm^{-2} is associated with the O-H stretching vibration, which indicates the presence of $Mg(OH)_2$ [54]. The peaks at 694, 607 and 551 cm^{-2} correspond to the O-H out-of-plane deformation vibration, and peak at 325 cm^{-2} to the O-H out-of-plane bending mode. The presence of C-H stretching vibration is related to the peak at 3079 cm^{-2}. The peaks at 1253, 1153 and 1036 cm^{-2} are identified as C-H in-plane bending vibration. The C=O bending vibration is related to 1323 cm^{-2}, while peaks at 1572, 1487 and 1375 cm^{-2} are matched with the ring C-C stretching vibration [54, 55]. A peak at 748 cm^{-2} is considered as ring in-plane bending mode. The peak at 990 cm^{-2} refers to the O=S=O stretching vibration [56]. Peaks associated with C-H in-plane vibration, C=O bending vibration, and O=S=O stretching vibration indicate the presence of species induced by complexing agents in the surface layer of the Mg anode during discharge at 10 mA cm^{-2}. The adsorption/deposition of these species on surface further amplifies the η_{ct} and η_{diff}, potentially leading to the sharp increase in discharge potential observed in mixtures at high current densities.

Thus, ethanol not only leads to the higher solution resistance, but also is inefficient in reducing the amount of discharge products formed on anode surface, which is detrimental to the discharge potential of anode. Single complexing agents effectively mitigate η_{ct} and η_{diff} resulting from discharge products, maintaining a low discharge potential across different current densities. Mixtures (SSA and ethanol, 3,4-DHB and ethanol) inhibit the deposition of discharge products at low current densities. However, the enhanced IR, $Mg(OH)_2$ and the adsorption/deposition of species (resulting in high η_{ct} and η_{diff}) collectively impede the continuous discharge process.

This hindrance contributes to the elevated discharge potential of Mg anode at 10 mA cm^{-2}.

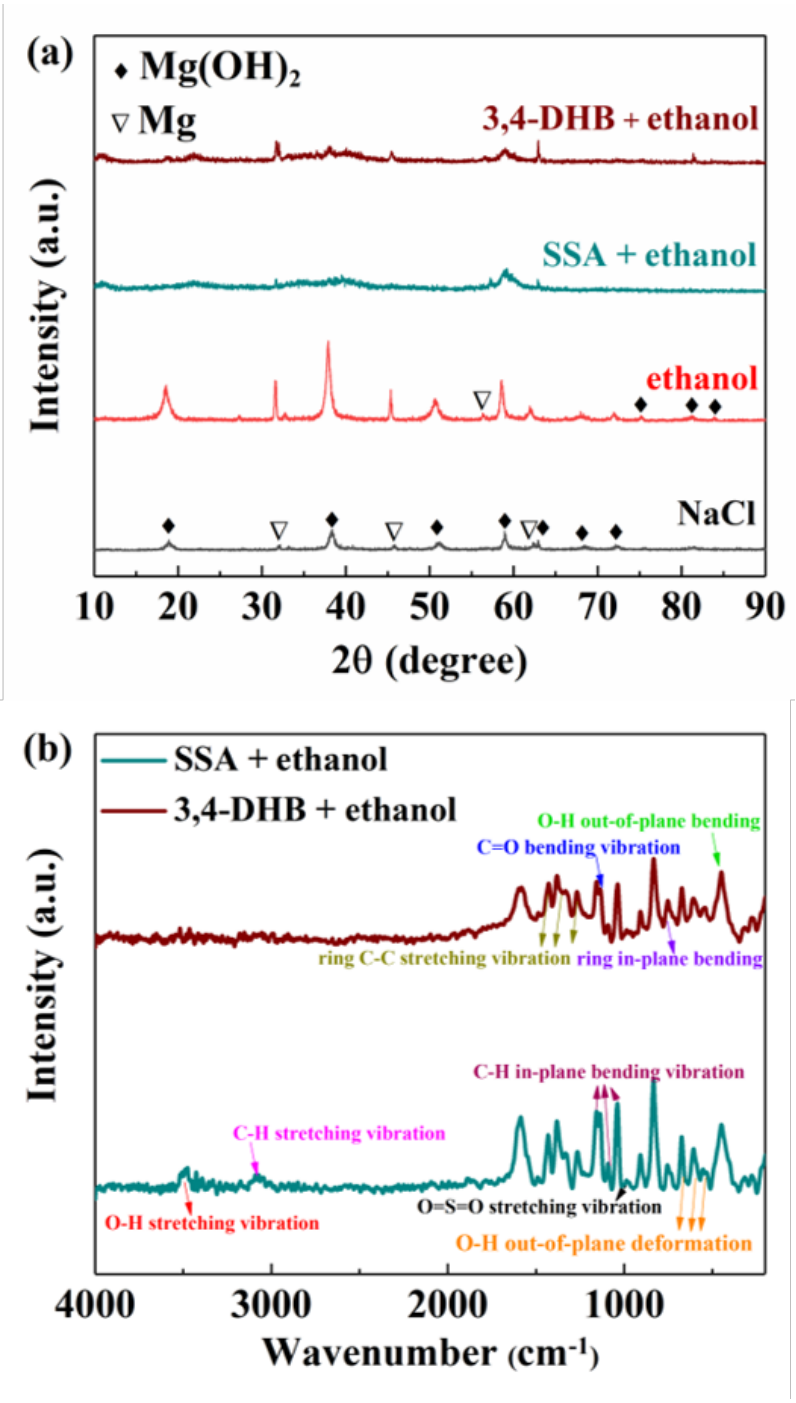

Fig. 6. Analysis of deposited discharge products in various electrolytes at 10 mA cm^{-2} for 10 h: (a) XRD spectra and (b) Raman spectra.

3.3. Full-cell battery test in various electrolytes

The discharge voltage curves of Mg-air battery in various electrolytes and current densities are depicted in Fig. 7. Since ethanol and two mixtures (SSA and ethanol, 3,4-

DHB and ethanol) electrolytes are hard to yield satisfactory results under high current densities in half-cell discharge, full-cell battery tests are conducted at low current densities.

The addition of ethanol to the electrolyte results in a lower discharge voltage compared to that in NaCl solution (Fig. 7a-c). Conversely, the presence of complexing agents leads to higher discharge voltages under low applied current densities. Obviously, the average discharge voltage of 1.57 V is achieved in the presence of Tiron (Fig. 7a and Table 2). However, with exception for Tiron, similar average discharge voltages are observed in NaCl solution and solutions containing single complexing agents at high current densities (Fig. 7c and Table 2).

In mixtures, Mg sample exhibits an average voltage of 1.47 V in the presence of Tiron and ethanol solution. Compared to blank solution, the Mg anode shows a similar discharge voltage when ethanol is added to solution containing SSA and 3,4-DHB (Fig. 7a and Table 2). However, as the current density increases, the Mg anode yields low discharge voltage in these mixtures. Notably, a discharge voltage of 0.81 V is observed in the presence of ethanol and 3,4-DHB, which is 0.51 V lower than that in NaCl solution at 5 mA cm^{-2} (Fig. 7b and Table 2). According to Equation 5, the power density of the anode depends on the average discharge voltage. Fig. 8 shows the power density of aqueous and ethanol-based battery in electrolytes with kinds of additives. Apparently, single ethanol decreases the power density of the Mg anode. At low current densities, the Mg anode exhibits high power density in the presence of complexing agents. Specifically, the power density of the anode increases from 3.53 to 3.93 mW cm^{-2} with the addition of Tiron. However, due to the decreased discharge voltage, complexing agents are ineffective at enhancing power density at high current densities. Compared to that in NaCl solution, Mg anode shows a slightly higher power density of 3.68 mW cm^{-2} in the Tiron and ethanol containing solutions. Mg anode also maintains a power density of 3.5 mW cm^{-2} in mixtures with SSA and 3,4 DHB. However, at high discharge current densities, the anode demonstrates low power density in these mixtures.

High solution resistance and the formation of discharge products lead to low electrochemical activity of the Mg anode. Additionally, the sluggish cathodic oxide reduction reaction (ORR) further decreases the discharge voltage [31]. Consequently, the Mg anode shows low discharge performance with the addition of ethanol at various current densities. Complexing agents significantly inhibit the deposition of discharge products, resulting in higher discharge voltage and power density. Due to low value of resistance of charge transfer, Mg anode demonstrates excellent discharge performance with addition of mixtures under low current densities. However, at high current densities, the combined effects of the discharge products on the surface, adsorbed/deposited additives, high solution resistance, and ORR collectively result in a low discharge voltage of anode in mixtures.

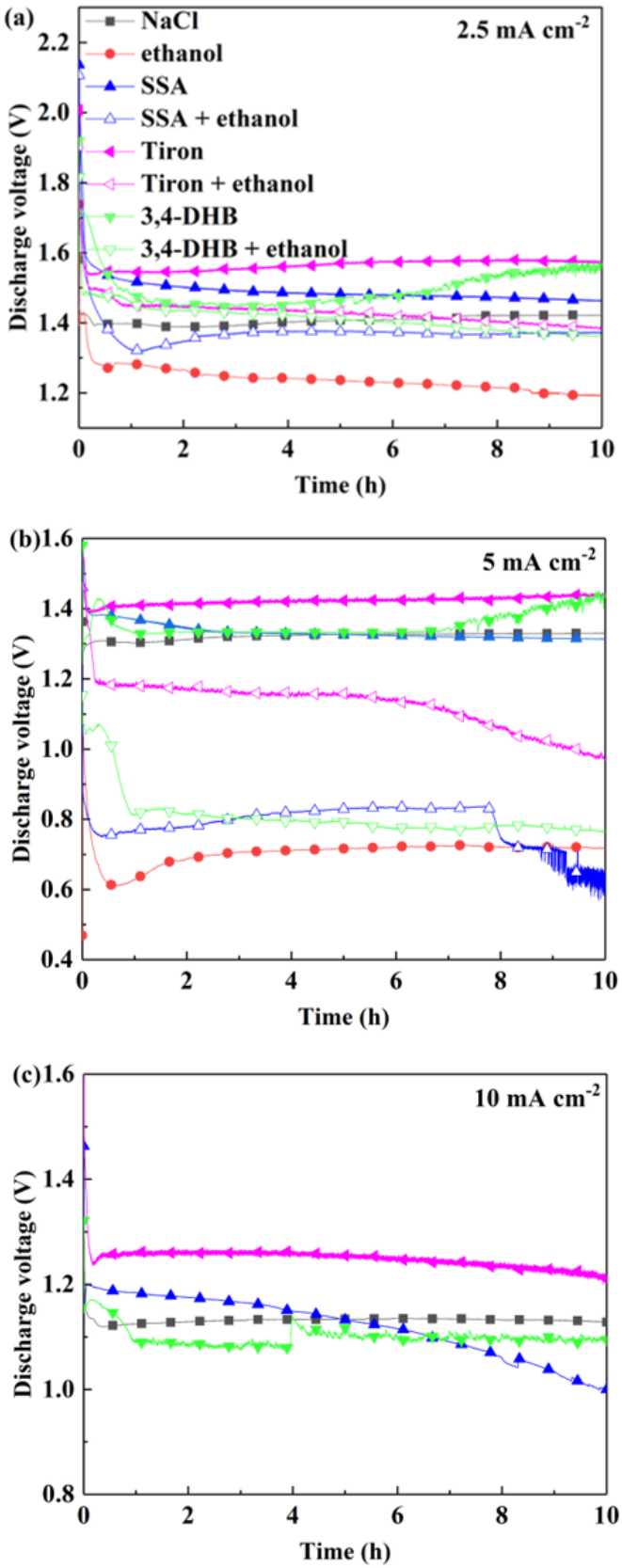

Fig. 7. Discharge voltage profiles of Mg-air battery at different current densities: (a) 1 mA cm^{-2}, (b) 2.5 mA cm^{-2} and (c) 5 mA cm^{-2} and (d) 10 mA cm^{-2} in various electrolytes.

Table 2. Electrochemical behavior of anodes in various electrolytes at different current densities in half cell and full cell.

	Electrolyte	NaCl	NaCl + ethanol	NaCl + SSA	Mix NaCl + SSA + ethanol	NaCl + 3,4-DHB	Mix NaCl + 3,4-DHB + ethanol	NaCl + Tiron	Mix NaCl + Tiron + ethanol
					Average discharge potential (vs. SCE) in half cell				
current density mA cm^{-2}	0 (OCP)	-1.66	-1.72	-1.86	-1.85	-1.86	-1.91	-1.94	-1.96
	2.5	-1.62	-1.61	-1.8	-1.68	-1.83	-1.67	-1.92	-1.9
	5	-1.61	-1.59	-1.71	-1.61	-1.73	-1.62	-1.87	-1.83
	10	-1.59	-1.53	-1.62	-	-1.63	-	-1.79	-1.77
					Average discharge voltage (V) in full cell				
current density mA cm^{-2}	2.5	1.41	1.24	1.49	1.39	1.5	1.4	1.57	1.47
	5	1.32	0.71	1.35	0.81	1.35	0.81	1.42	1.13
	10	1.13	-	1.11	-	1.11	-	1.25	-

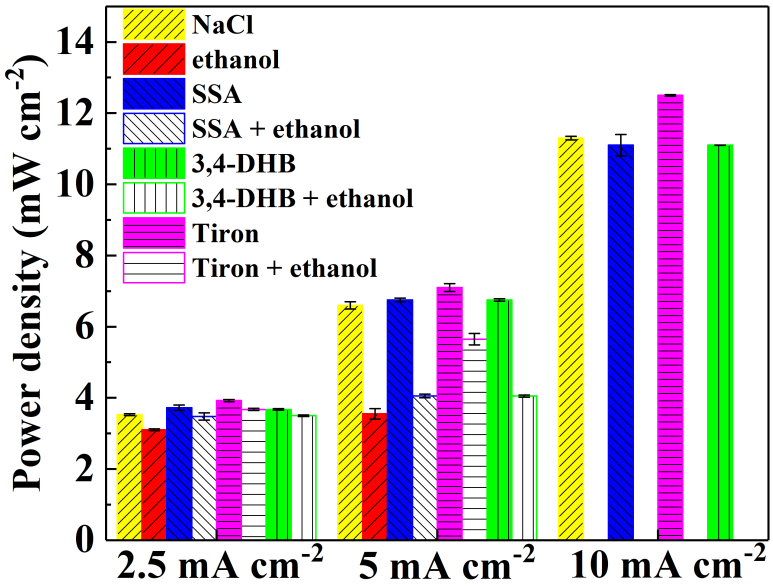

Fig. 8. Power density of Mg in NaCl solutions with and without additives.

3.4. Actual anode weight loss during discharge

Fig. 9 and Table 3 shows the discharge performance of specimen in various electrolytes. It can be seen that the utilization efficiency of anode is slightly increased in ethanol containing solution (Fig. 9a and Table 3). However, as the current density increases to 5 mA cm^{-2}, ethanol fails to enhance the discharge performance of the anode, decreasing the utilization efficiency by 2.2% (Fig. 9a and Table 3). The addition of single complexing agents significantly reduces the utilization efficiency and specific capacity of the anode at low current densities. In the presence of Tiron, the Mg anode achieves only 12.1% utilization efficiency (Fig. 9a and Table 3). Similarly, 3,4-DHB decreases the specific capacity of the anode from 1210.8 to 511.7 mAh g^{-1} (Fig. 9b and Table 3). In contrast to ethanol, the Mg anode demonstrates high discharge performance with addition of single complexing agents at high current densities. Notably, SSA enhances these two parameters of Mg anode to 61.3% and 1384.8 mAh g^{-1} at 5 mA cm^{-2}, respectively (Fig. 9a, b and Table 3). At 10 mA cm^{-2}, the Mg anode shows the highest utilization efficiency in the 3,4-DHB containing solution among various solutions, reaching 66.7% (Fig. 9a and Table 3).

The Mg anode demonstrates superior utilization efficiency and specific capacity in the presence of mixtures, except for Tiron-containing solution. Notably, the utilization

efficiency of 85.7% is achieved in a mixture of 3,4-DHB and ethanol, which is 32.7% higher than the blank NaCl solution (Fig. 9a and Table 3). Mixtures of SSA and ethanol, and 3,4-DHB and ethanol, continue to significantly enhance the utilization efficiency of samples (5 mA cm^{-2}). At 10 mA cm^{-2} of current density, Mg anode shows higher discharge performance in a mixture of Tiron and ethanol in compared to the NaCl-based solution. However, it has been observed that a sharp increase of average potential occurs in mixtures of SSA and ethanol, and 3,4-DHB and ethanol at 10 mA cm^{-2}, indicating that these two mixtures are unsuitable for use at high current densities (Fig. 4d). Therefore, calculating these two parameters of anode in these mixtures at this current density is meaningless.

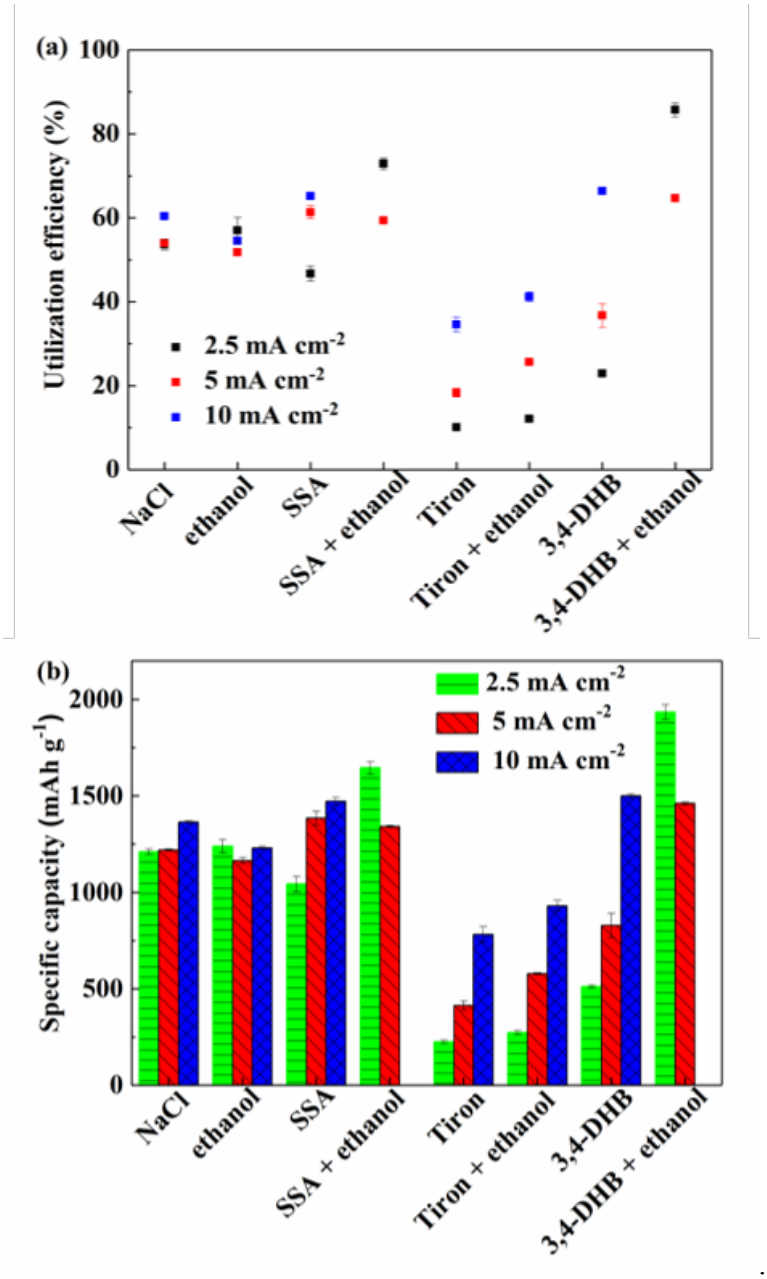

Fig. 9. Discharge behaviour of specimen in solutions with kinds of additive: (a) utilization efficiency (%) and (b) specific capacity (mAh g^{-1}).

Table 3. Utilization efficiency and specific capacity of anodes in various electrolytes at different current densities.

	Current density (mA cm^{-2})	NaCl	NaCl + ethanol	NaCl + SSA	Mix NaCl + SSA + ethanol	NaCl + 3,4-DHB	Mix NaCl + 3,4-DHB + ethanol	Tiron	Mix NaCl + Tiron + ethanol
Utilization efficiency (%)	2.5	53.6±1.2	57±3	46.7±1.8	72.9±1.4	22.9±0.3	85.7±1.7	10.1±0.4	12.1±0.5
	5	54±0.2	51.8±0.7	61.3±1.6	59.4±0.3	36.7±2.8	64.7±0.3	18.3±1	25.6±0.2
	10	60.4±0.3	54.5±0.4	65.2±0.9	-	66.4±0.5	-	34.6±1.8	41.2±1.2
Specific capacity (mAh g^{-1})	2.5	1210.8±13.5	1240.1±33.5	1043.4±40.3	1646.8±31.6	511.7±6.8	1935.9±38.4	225.6±9.1	273.3±11.3
	5	1219.9±4.5	1164.5±15.8	1384.8±36.1	1341.8±6.8	829±63.3	1456.6±6.8	413.4±22.6	578.3±4.5
	10	1364.4±6.8	1231.1±9	1472.9±20.3	-	1499.9±11.3	-	781.6±40.7	930.7±27.1

The actual weight loss ΔW during the discharge test can be represented by Equation 6 [28].

$$\Delta W = \Delta W_{theo} + \Delta W_{self-corr} + \Delta W_{chunk\ effect} \quad (12)$$

ΔW_{theo} represents the theoretical weight loss associated with the electronic transport, $\Delta W_{self-corr}$ corresponds to anode weight loss resulted from self-corrosion process during discharge, while $\Delta W_{chunk\ effect}$ is related to the undissolved Mg substrate surrounded by discharge products. It is apparent that low $\Delta W_{self-corr}$ and $\Delta W_{chunk\ effect}$ determine the high utilization efficiency.

Real-time hydrogen tests during discharge are employed to investigate the self-corrosion rate of the anode in different electrolytes (Fig. 10). After extended discharge tests, undissolved Mg matrix appears in the discharge products (chunk effect). This undissolved Mg matrix, surrounded by discharge products, can detach from the sample and lead to increase of H_2 evolution and weight loss ($\Delta W_{self-corr}$). Therefore, 6 h of discharge at 2.5 and 5 mA cm^{-2}, and 4 h at 10 mA cm^{-2}, are used to evaluate the actual self-corrosion rate.

At 2.5 mA cm^{-2}, ethanol reduces the H_2 volume from 6 to 3.65 mL cm^{-2} (Fig. 10a). However, Mg anode shows a higher released H_2 volume in solutions containing complexing agents containing compared to NaCl solution at low current density. It is worth to be mentioned that lower H_2 volume is demonstrated in mixtures, especially in 3,4-DHB and ethanol solution with 3.15 mL cm^{-2} of H_2 after discharge for 6 h (Fig. 10a). At a current density of 5 mA cm^{-2} (Fig. 10b), the H_2 volume in NaCl solution with added ethanol is similar to that in pure NaCl solution. Complexing agents lead to a high release of H_2 volume during discharge, indicating a high self-corrosion rate. In contrast, Mg samples exhibit low H_2 volume in mixtures, as shown of 6.1 mL cm^{-2} (Fig. 10b) with addition of 3,4-DHB and ethanol. When current density increases to high value (Fig. 10c), ethanol and mixtures increase the H_2 release rate during discharge. However, except for Tiron, complexing agents significantly inhibit H_2 evolution. The H_2 volume in the presence of 3,4-DHB is 1.35 mL cm^{-2}.

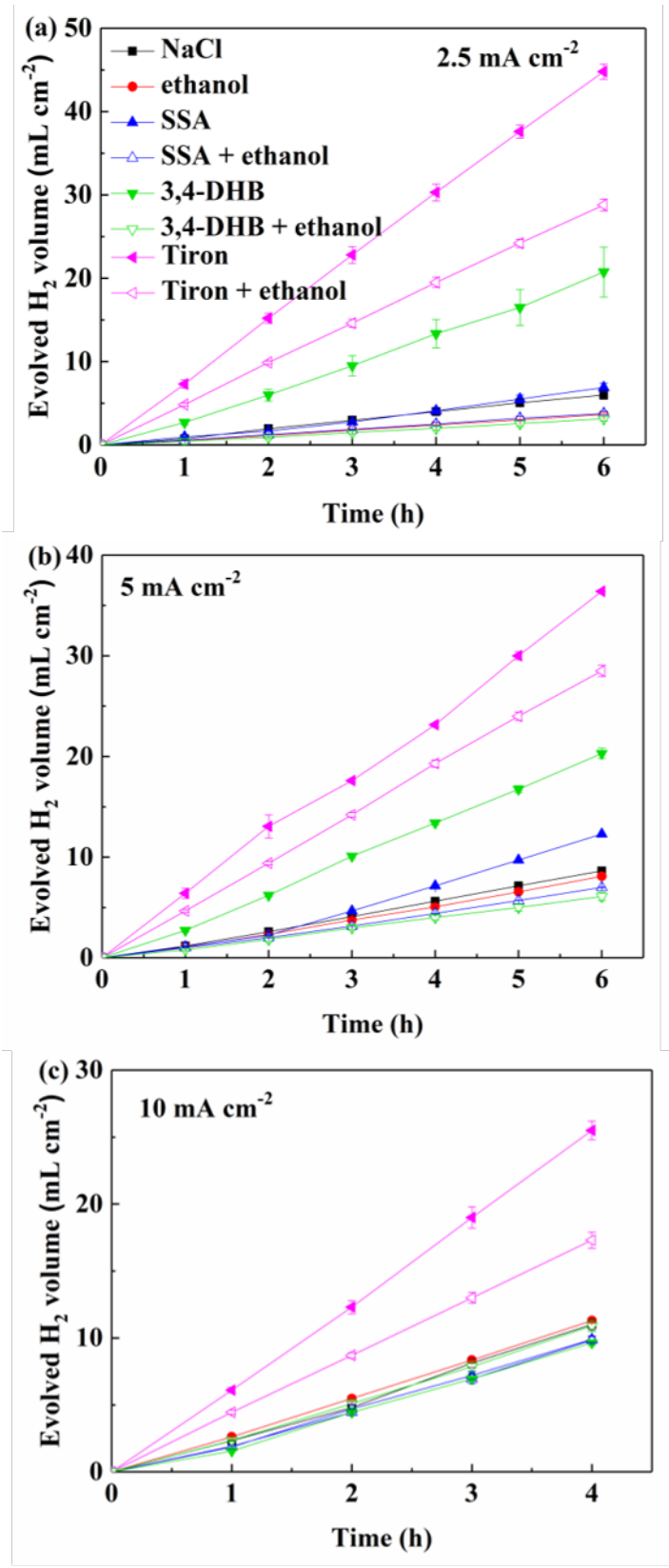

Fig. 10. Real-time hydrogen evolution measurements of Mg sample during discharge at (a) 2.5 mA cm^{-2}, (b) 5 mA cm^{-2} and (c) 10 mA cm^{-2} in NaCl solution with different additives.

The cross-sectional morphology of specimen after discharge in different solutions for 10 h is demonstrated in Fig. 11. The discharge products with chunk effect are shown on surface in NaCl and ethanol-based solutions (Fig. 11a, b, e and f). Then, the chunk effect is hardly visible on Mg surfaces with the addition of complexing agents. At low current densities, the chunk effect is unobserved in mixtures (Fig. 11c, i and j). However, at 5 mA cm^{-2}, the introduction of ethanol into solutions containing 3,4-DHB and SSA results in deposition of discharge products on the anode surface (Fig. 11g and o) and apparent chunk effect.

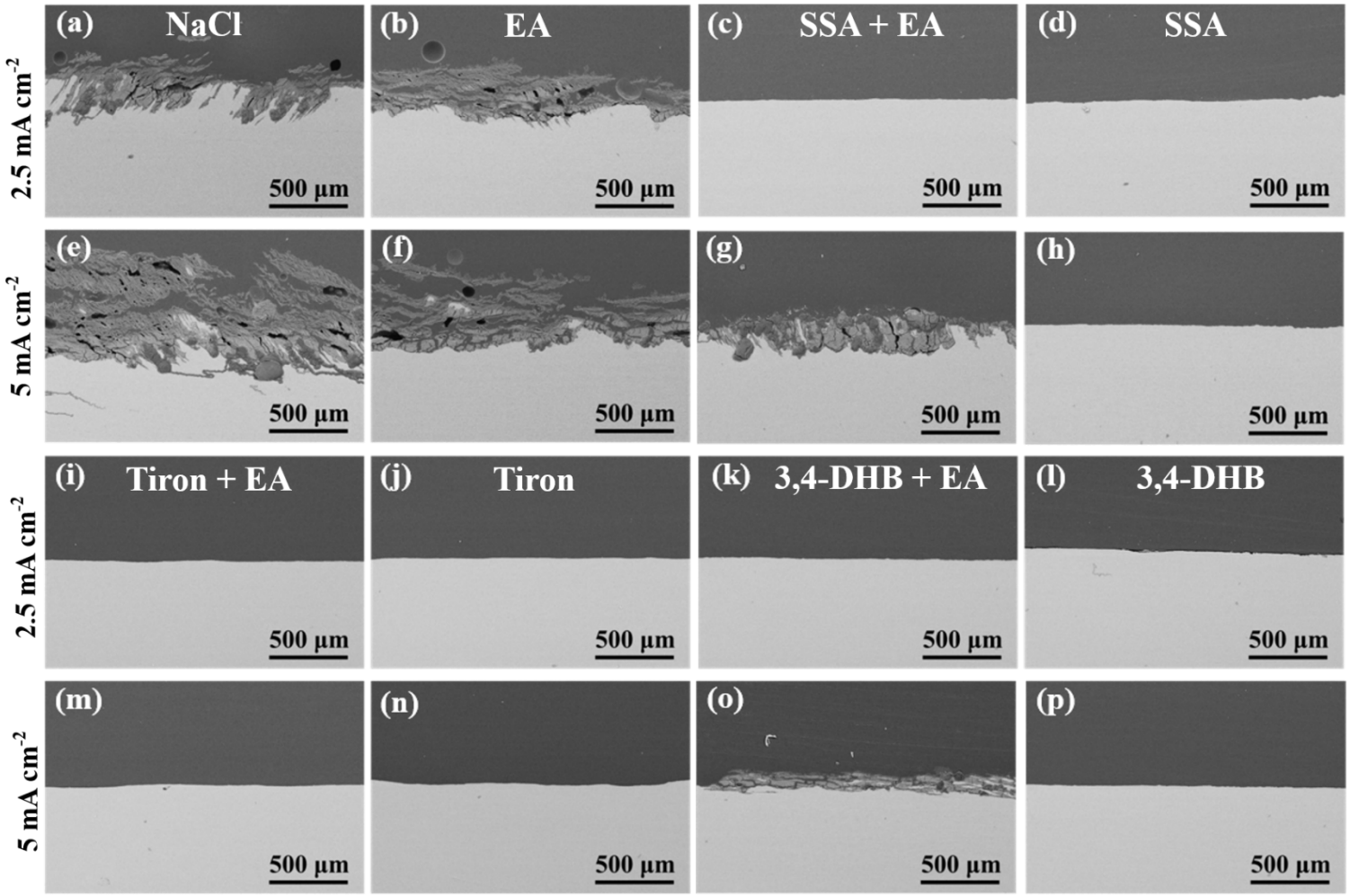

Fig. 11. Cross-sectional SEM images of discharged specimen at different current densities in various electrolytes.

Real-time hydrogen test reflects the weight loss as it is deduced from $\Delta W_{self-corr}$. The presence of ethanol reduces $\Delta W_{self-corr}$ at low current densities, while accelerates the self-corrosion rate of anode as current density increases. Large $\Delta W_{self-corr}$ contributes to the low utilization efficiency in solutions with complexing agents at low current density. However, single complexing agents reduce the $\Delta W_{chunk\ effect}$ across different current densities. Moreover, $\Delta W_{self-corr}$ caused by SSA and 3,4-DHB is significantly reduced at 10 mA cm^{-2}, leading to high discharge performance of the anode. In the case of mixture solutions (SSA and ethanol, 3,4-DHB and ethanol), they not only reduce the evolved H_2 volume during discharge, but also suppress the appearances of discharge products. Therefore, both $\Delta W_{self-corr}$and $\Delta W_{chunk\ effect}$ are inhibited in the presence of mixtures at 2.5 mA cm^{-2}, greatly enhancing the discharge performance of anode (3,4-DHB and ethanol, SSA and ethanol). However, at high current density, these two factors (high self-corrosion rate of sample and severe chunk effect) result in the low discharge performance of the Mg anode.

In order to understand the decreased evolution of H_2 and improved utilization efficiency of Mg anode in electrolytes with ethanol and mixtures at 2.5 mA cm^{-2}, ToF-SIMS negative ion depth profiles are employed to investigate the surface film layers formed on the Mg anode after 5 min of discharge (Fig. 12). Different ion intensities reflect various chemical compositions of the surface layers [37]. MgO^-, $MgOH^-$, MgH^- and $MgCO_3$ ions correspond to MgO, $Mg(OH)_2$ and $MgCO_3$, respectively. The S^- signal represents SSA adsorbed on the Mg surface in SSA and ethanol containing solution. The 80 % of maximum intensity of MgO^- signal is set to evaluate the thickness of the surface layer [32, 57]. Assuming the sputtering rate of 0.1 nm/s, the thickness of total oxide-hydroxide layer was calculated and it shows a decrease in the following order: NaCl (51 nm) > ethanol (40 nm) > 3,4-DHB and ethanol (35 nm) > SSA and ethanol (28 nm) [37]. These mixtures, i.e. 3,4-DHB with ethanol and SSA with ethanol, significantly inhibit the growth of the surface layer compared to the NaCl electrolyte.

The $MgOH^-$ signal reaches its maximum intensity first in the blank NaCl solution (Fig. 12a), indicating that the outer surface layer primarily consists of $Mg(OH)_2$. Subsequently, the MgO^- signal exhibits maximum intensity after the $MgOH^-$ signal,

indicating that MgO contributes to the formation of the inner layer. A similar distribution of hydroxide and oxide is observed in ethanol-based electrolyte (Fig. 12b). However, it is noteworthy that the mixtures influence the distribution of the hydroxide and oxide layers. In the SSA and ethanol (Fig. 12c), 3,4-DHB and ethanol electrolytes (Fig. 12d), the maximum intensity of hydroxide ($MgOH^-$) coincides almost exactly with that of the oxide (MgO^-), indicating the formation of a more mixed oxide-hydroxide layer. Additionally, the maximum intensity of S^- appears before the peaks of MgO^- and the Mg^{2-} signals in the SSA and ethanol-containing solutions (Fig. 12c). This suggests that S-containing species are prone to depositing in the outer surface layer during discharge.

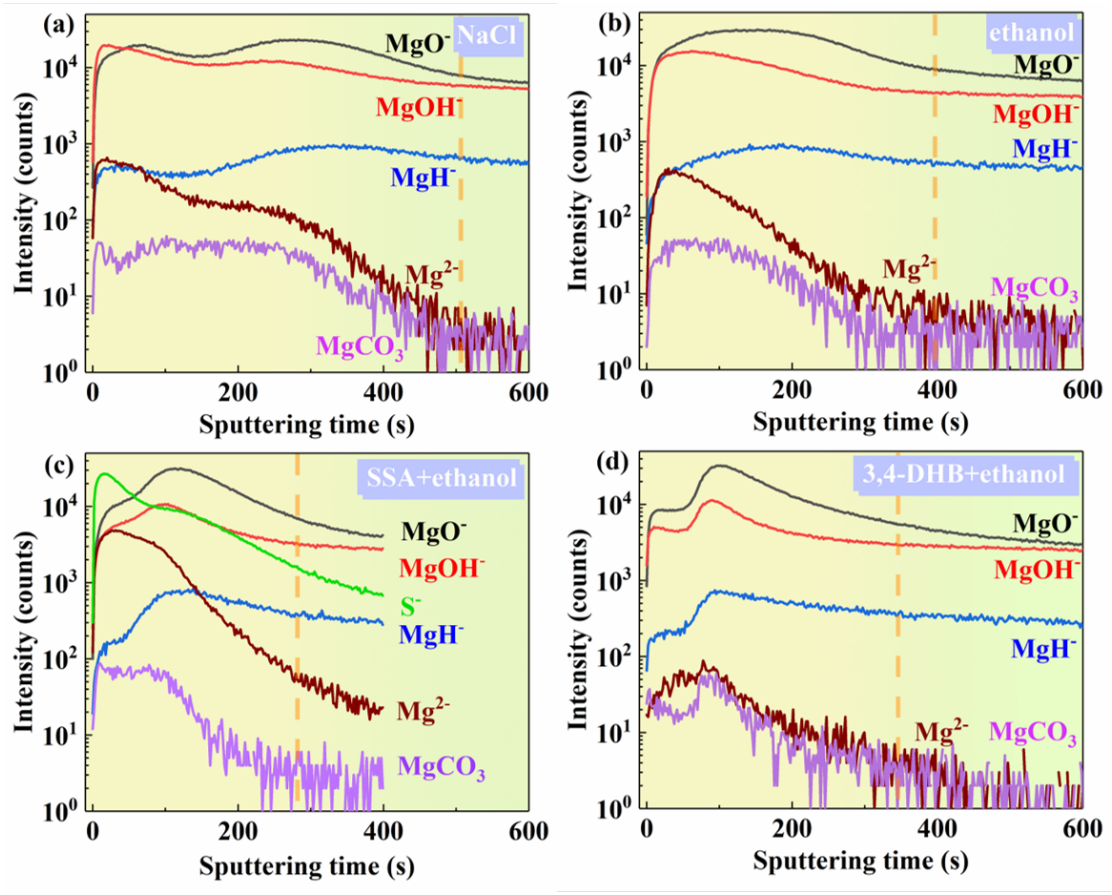

Fig. 12. ToF-SIMS negative in-depth ion profiles of discharge product layer after 5 min-discharge in NaCl solution with and without electrolyte additives at current density of 2.5 mA cm^{-2}.

To gain better insight into the chemical modifications of the surface layer, the ratio of $MgOH^-$ to MgO^- is presented in Fig. 13. Initially, these ratios decrease and then increase with sputtering time, indicating different compositions of the outer and inner surface layers in various solutions. The highest content of hydroxide deposit (2.15 for $MgOH^-$ to MgO^- ratio) in the outer surface layer is evident in the reference. In solution with ethanol, the reduction of the $MgOH^-$ to MgO^- ratio in the outer and inner layer can be observed, implying an enrichment in MgO. Notably, mixtures significantly influence the ratio of $MgOH^-$ to MgO^- in the outer surface layer. The ratios decrease to around 0.25 in mixtures with 3,4-DHB and SSA, indicating a substantial restriction on the growth of hydroxide in the outer layer.

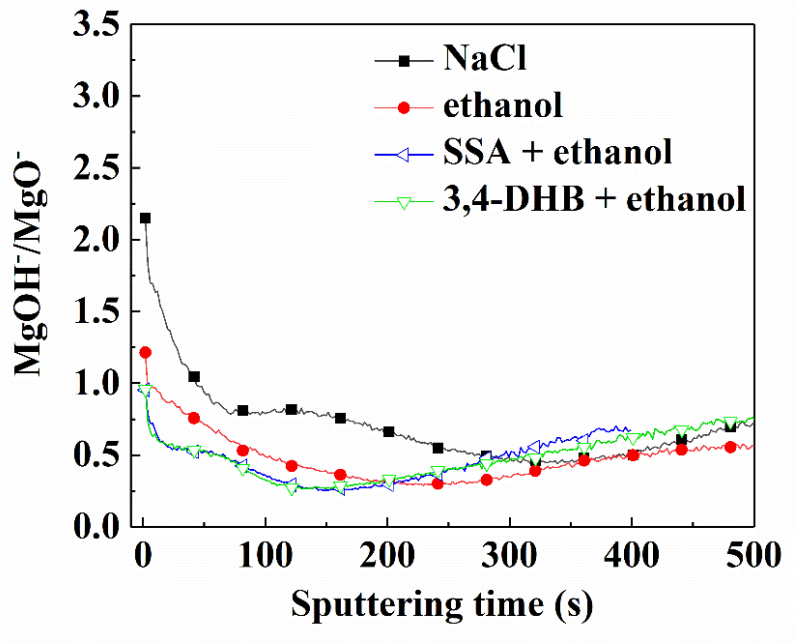

Fig. 13. Ratio of $MgOH^-$ and MgO^- in deposited surface layer after discharge at 2.5 mA cm^{-2} for 5 min in various solutions.

In summary, the mixtures facilitate the formation of a surface layer enriched in MgO, reducing the contact area between H^+ and Mg substrate and inhibiting self-corrosion. Additionally, electrolyte additives are effective in preventing the excessive deposition of $Mg(OH)_2$ on surface, significantly reducing the cathodic sites (dark regions) for HER [58-60]. This is reflected by the low self-corrosion rate observed during discharge in ethanol and mixture solutions. Interestingly, the Mg anode exhibits lower H_2 evolution

in mixtures compared to ethanol-containing solutions. As seen in Fig. 12c and d, a relatively thin layer deposits on the surface in mixtures compared to other solutions. S-containing species are clearly observed in the outer surface layer of the Mg surface in SSA and ethanol solution. Moreover, the ratio of $MgOH^-$ to MgO^- confirms that the outer layer consists has a high portion of MgO in the presence of mixtures. This MgO rich layer blocks the cathodic sites and inhibits the continuous growth of the hydroxide-rich layer on the surface. The presence of S-like species and high content of MgO together form a compact layer, resulting in the lowest HER of the anode in mixtures among these electrolytes during discharge.

4. Discussion

In the present work, the influence of various additives on the electrochemical performance of Mg sample is systematically studied by means of electrochemical tests and surface analysis. Ethanol reduces the free H^+ in the electrolyte and leads to high solution resistance, which is detrimental to discharge voltage. At low current densities, addition of ethanol results in the formation of an oxide-rich inner surface layer, restricting the reaction between H^+ and Mg matrix during discharge. Furthermore, ethanol inhibits the formation of $Mg(OH)_2$ on surface, reducing the cathodic sites for HER. Thus, high utilization efficiency of Mg anode with addition of ethanol is achieved at low current densities. As current density increases, discharge products tend to deposit on surface as demonstrated in Fig. 5f. Large amounts of $Mg(OH)_2$ on the surface act as strong local cathodes, significantly increasing HER during the discharge process [58]. Consequently, undissolved Mg matrix appears in discharge products on surface, which detaches from Mg sample without actual charge transfer [15, 18]. This large weight loss of self-corrosion process and chunk effect leads to low discharge performance.

Fig. 14 shows thermodynamic equilibrium diagram of the electrolyte after discharge in solutions containing complexing agents, simulated by Hydra/Medusa® software. Clearly, the pH of $Mg(OH)_2$ formation is set at 9.4 after discharge in reference (Fig. 14a). The pH for the accumulation of discharge products increases to 11.4 and 11.6

with addition of SSA and 3,4-DHB, respectively (Fig. 14b and c). It should be noted that Tiron hinders the formation of $Mg(OH)_2$ on the Mg surface, as depicted by the presence of Mg^{2+} complex ($MgC_6H_3O_8S_2$) in the electrolyte (Fig. 14d).

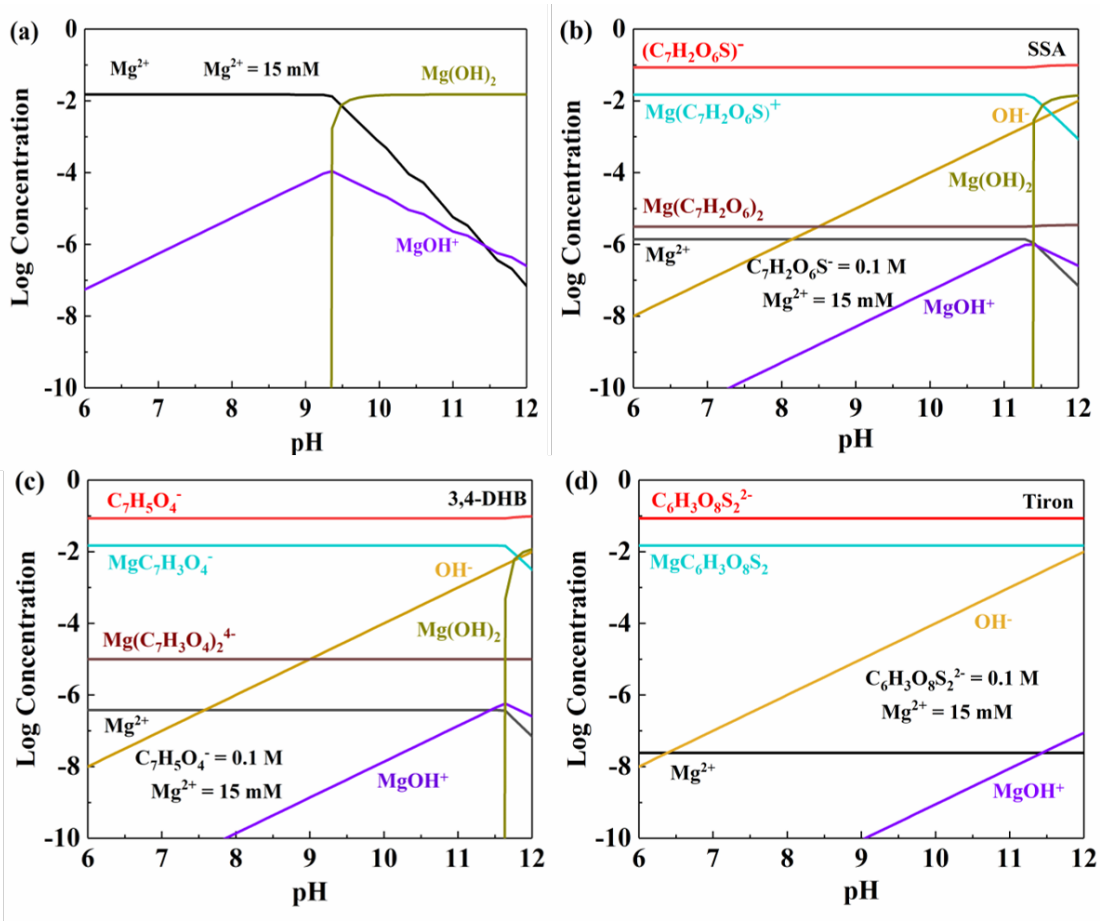

Fig. 14. Thermodynamic calculation of the solution composition and precipitation species formed upon Mg discharge in (a) NaCl, (b) SSA, (c) 3,4-DHB and (d) Tiron.

The deposition of discharge products significantly reduces the contact area between the anode and the electrolyte, which is detrimental to the continuous discharge process. Complexing agents chelate with Mg^{2+} and inhibit the accumulation of discharge products, leading to high discharge voltage and power density. However, strong complexing agents facilitate the dissolution process, resulting in a large volume of released H_2 during discharge at low current density. Strong HER is observed in the presence of complexing agents, causing significant weight loss ($\Delta W_{self-corr}$).

However, at high current densities of 10 mA cm^{-2} (Fig. 10c), SSA and 3,4-DHB reduces the H_2 evolution in comparison to blank NaCl solution due to lower quantity of discharge products ($Mg(OH)_2$) acting as cathodic sites which promote the dissolution process HER [58]. Thus, these two complexing agents are capable of reducing the cathodic effects caused by discharge products, thereby decreasing the self-corrosion rate of the anode and greatly suppressing the chunk effect. The reduced weight loss induced by $\Delta W_{self-corr}$ and $\Delta W_{chunk\ effect}$, determines the high values of two parameters of anode in solutions with single complexing agent at high current densities. The introduction of ethanol into solutions containing complexing agents greatly reduces the conductivity of water-based electrolyte, which means that transfer rate of species, e.g. complexes, ($Mg(C_7H_2O_6S)^+$, $Mg(C_7H_3O_4)^-$ and $Mg(C_7H_3O_4)_2^{4-}$) are reduced. These species prefer to deposit/absorb into the surface layer instead of dissolving into the electrolytes, as evidenced by the deposition of S-like species detected by ToF-SIMS. However, mixtures still have the ability to reduce the amount of discharge products on surface at low current densities. Therefore, the similar discharge voltage and power density of the anode is maintained compared to that in blank NaCl solution. With the increase of current density, large η_{ct} and η_{diff} caused by discharge products, adsorbed/deposited complexes and high IR together lead to the low discharge voltage and power density of the anode. Regarding utilization efficiency and specific capacity, complexes adsorb/deposit in the outer surface layer, which further reduces the area exposed to electrolyte and hinders the growth of hydroxide-rich layer on surface. A thin surface layer, consisting of complexes and MgO, inhibits the HER during discharge, leading to low weight loss from the self-corrosion process. Low weight loss of $\Delta W_{self-corr}$ and $\Delta W_{chunk\ effect}$ synergistically results in a relatively high utilization efficiency in mixtures at low current densities. However, mixtures are insufficient to chelate large amounts of generated Mg^{2+} at high current density. Therefore, large amounts of discharge products, deposit on surface and form local cathodic sites, which increase the self-corrosion rate of the anode. At the same time, the chunk effect is

evident in discharge products and detaches into the electrolytes, further reducing the actual mass loss of Mg anode.

5. Conclusions

(1) A mixture of 30 vol% ethanol and 0.1 M complexing agent has been utilized for the first time as the electrolyte in Mg-air battery. Mg anode shows great discharge performance in NaCl solution with 30 vol% ethanol and 0.1 M 3,4-DHB, achieving utilization efficiency of 85.7%.

(2) 30 vol% ethanol reduces the free H^+ and promotes the formation of double surface layer (hydroxide outer layer and oxide-rich inner layer). However, in the mixtures the mixed oxide-hydroxide layer with a decreased quantity of hydroxide can be observed. This type of layer hinders the formation of cathodic sites and decreases of self-corrosion rate of anode.

(3) The adsorption/deposition of complexes in outer surface layer inhibits the growth of hydroxide-rich layer. The thin surface layer, primarily composed of complexes and MgO, along with the inhibited chunk effect, result in the highest utilization efficiency and specific capacity of Mg anode among various solutions.

Author Contributions

Yuxin Zhou: Conceptualization, Methodology, Investigation, Writing- Original draft preparation. Xiaopeng Lu: Conceptualization, Investigation, Writing- Reviewing and Editing, Supervision, Funding acquisition. Jolanta Światowska: Conceptualization, Supervision, Data curation, Writing- Reviewing and Editing. Antoine Seyeux: Formal analysis, Data curation. Fuhui Wang: Writing- Reviewing and Editing, Supervision, Funding acquisition.

Acknowledgements

This work was financially supported by the National Key R&D Program of China (No. 2023YFB3809502), National Natural Science Foundation of China (No. 52071067), Shenyang Young and Middle-aged Science and Technology Innovation Talent Support Program (RC231178) and the Fundamental Research Funds for the Central Universities (N2302019). Région île-de-France is acknowledged for partial funding of the ToF-

SIMS equipment. Yuxin Zhou is grateful to the China Scholarship Council (CSC) for funding (No. 202306080126).

Conflicts of interest or competing interests

The authors declare that they have no known competing financial interests or personal relationships that could have appeared to influence the work reported in this paper.

References

[1] M. Deng, L. Wang, D. Höche, S.V. Lamaka, D. Snihirova, P. Jiang, M.L. Zheludkevich, Corrosion and discharge properties of Ca/Ge micro-alloyed Mg anodes for primary aqueous Mg batteries, Corrosion Science, 177 (2020).

[2] S.-m. Cheng, W.-l. Cheng, X.-j. Gu, H. Yu, Z.-F. Wang, H.-x. Wang, L.-f. Wang, Discharge properties of low-alloyed Mg–Bi–Ca alloys as anode materials for Mg–air batteries: Influence of Ca alloying, Journal of Alloys and Compounds, 823 (2020).

[3] X. Chen, Y. Jia, Z. Shi, Q. Le, J. Li, M. Zhang, M. Liu, A. Atrens, Understanding the discharge behavior of an ultra-high-purity Mg anode for Mg–air primary batteries, Journal of Materials Chemistry A, 9 (2021) 21387-21401.

[4] X. Chen, Q. Zou, Q. Le, M. Zhang, M. Liu, A. Atrens, Influence of heat treatment on the discharge performance of Mg-Al and Mg-Zn alloys as anodes for the Mg-air battery, Chemical Engineering Journal, 433 (2022) 133797.

[5] M.A. Deyab, Decyl glucoside as a corrosion inhibitor for magnesium–air battery, Journal of Power Sources, 325 (2016) 98-103.

[6] M. Jiang, H. He, W.-J. Yi, W. Huang, X. Pan, M.-Y. Wang, Z.-S. Chao, ZIF-67 derived Ag-Co 3 O 4 @N-doped carbon/carbon nanotubes composite and its application in Mg-air fuel cell, Electrochemistry Communications, 77 (2017) 5-9.

[7] H. Xiong, K. Yu, X. Yin, Y. Dai, Y. Yan, H. Zhu, Effects of microstructure on the electrochemical discharge behavior of Mg-6wt%Al-1wt%Sn alloy as anode for Mg-air primary battery, Journal of Alloys and Compounds, 708 (2017) 652-661.

[8] D. Hoche, S.V. Lamaka, B. Vaghefinazari, T. Braun, R.P. Petrauskas, M. Fichtner, M.L. Zheludkevich, Performance boost for primary magnesium cells using iron

complexing agents as electrolyte additives, Sci Rep, 8 (2018) 7578.

[9] X. Liu, S. Liu, J. Xue, Discharge performance of the magnesium anodes with different phase constitutions for Mg-air batteries, Journal of Power Sources, 396 (2018) 667-674.

[10] M. Deng, D. Höche, S.V. Lamaka, L. Wang, M.L. Zheludkevich, Revealing the impact of second phase morphology on discharge properties of binary Mg-Ca anodes for primary Mg-air batteries, Corrosion Science, 153 (2019) 225-235.

[11] D. Kurchavov, M. Haddad, V. Lair, P. Volovitch, Mg-alloys in water – hydrophilic ionic liquid mixtures: Is there a negative difference effect?, Corrosion Science, 200 (2022) 110178.

[12] J. Ma, Y. Zhang, M. Ma, C. Qin, F. Ren, G. Wang, Corrosion and discharge performance of a magnesium aluminum eutectic alloy as anode for magnesium–air batteries, Corrosion Science, 170 (2020).

[13] D. Huang, F. Cao, T. Ying, D. Zheng, G.-L. Song, High-energy-capacity metal-air battery based on a magnetron-sputtered Mg–Al anode, Journal of Power Sources, 520 (2022) 230874.

[14] Y. Zhou, X. Lu, M.L. Zheludkevich, F. Wang, Tailoring corrosion and discharge performance of Mg anode by corrosion inhibitor, Electrochimica Acta, 436 (2022) 141471.

[15] M. Deng, L. Wang, D. Höche, S.V. Lamaka, D. Snihirova, B. Vaghefinazari, M.L. Zheludkevich, Clarifying the decisive factors for utilization efficiency of Mg anodes for primary aqueous batteries, Journal of Power Sources, 441 (2019).

[16] N. Wang, Y. Mu, W. Xiong, J. Zhang, Q. Li, Z. Shi, Effect of crystallographic orientation on the discharge and corrosion behaviour of AP65 magnesium alloy anodes, Corrosion Science, 144 (2018) 107-126.

[17] C. Gong, X. He, D. Fang, B. Liu, X. Yan, Effect of second phases on discharge properties and corrosion behaviors of the Mg-Ca-Zn anodes for primary Mg-air batteries, Journal of Alloys and Compounds, 861 (2021).

[18] M. Deng, L. Wang, D. Höche, S.V. Lamaka, P. Jiang, D. Snihirova, N. Scharnagl, M.L. Zheludkevich, Ca/In micro alloying as a novel strategy to simultaneously enhance power and energy density of primary Mg-air batteries from anode aspect, Journal of Power Sources, 472 (2020).

[19] J. Sha, M. Qiao, J. Bao, H. Liu, S. Yin, W. Liu, Z. Zhao, Z. Zhao, J. Cui, Z. Zhang, Improving the electrochemical behaviors and discharge performance of as-rolled Mg-4Li alloys through multicomponent alloying, Journal of Alloys and Compounds, 895 (2022) 162536.

[20] F.-e. Shangguan, W.-l. Cheng, Y.-h. Chen, Z.-q. Cui, H. Yu, H.-x. Wang, L.-f. Wang, H. Li, H. Hou, Role of micro-Ca/In alloying in tailoring the microstructural characteristics and discharge performance of dilute Mg-Bi-Sn-based alloys as anodes for Mg-air batteries, Journal of Magnesium and Alloys, (2022).

[21] F. Tong, X. Chen, S. Wei, J. Malmström, J. Vella, W. Gao, Microstructure and battery performance of Mg-Zn-Sn alloys as anodes for magnesium-air battery, Journal of Magnesium and Alloys, 9 (2021) 1967-1976.

[22] X. Chen, H. Wang, Q. Zou, Q. Le, C. Wen, A. Atrens, The influence of heat treatment on discharge and electrochemical properties of Mg-Gd-Zn magnesium anode with long period stacking ordered structure for Mg-air battery, Electrochimica Acta, 367 (2021).

[23] B. Ma, C. Tan, L. Ouyang, H. Shao, N. Wang, M. Zhu, Microstructure and discharge performance of Mg-La alloys as the anodes for primary magnesium-air batteries, Journal of Alloys and Compounds, 918 (2022) 165803.

[24] Y. Zhao, G. Huang, C. Zhang, C. Peng, F. Pan, Effect of phosphate and vanadate as electrolyte additives on the performance of Mg-air batteries, Materials Chemistry and Physics, 218 (2018) 256-261.

[25] B. Vaghefinazari, D. Höche, S.V. Lamaka, D. Snihirova, M.L. Zheludkevich, Tailoring the Mg-air primary battery performance using strong complexing agents as electrolyte additives, Journal of Power Sources, 453 (2020).

[26] L. Wang, D. Snihirova, M. Deng, B. Vaghefinazari, S.V. Lamaka, D. Höche, M.L. Zheludkevich, Tailoring electrolyte additives for controlled Mg-Ca anode activity in aqueous Mg-air batteries, Journal of Power Sources, 460 (2020).

[27] L. Wang, D. Snihirova, M. Deng, C. Wang, D. Höche, S.V. Lamaka, M.L. Zheludkevich, Indium chloride as an electrolyte additive for primary aqueous Mg batteries, Electrochimica Acta, 373 (2021).

[28] L. Wang, D. Snihirova, M. Deng, B. Vaghefinazari, D. Höche, S.V. Lamaka, M.L. Zheludkevich, Enhancement of discharge performance for aqueous Mg-air batteries in 2,6-dihydroxybenzoate-containing electrolyte, Chemical Engineering Journal, 429 (2022) 132369.

[29] Y. Yan, D. Gunzelmann, C. Pozo-Gonzalo, A.F. Hollenkamp, P.C. Howlett, D.R. MacFarlane, M. Forsyth, Investigating discharge performance and Mg interphase properties of an Ionic Liquid electrolyte based Mg-air battery, Electrochimica Acta, 235 (2017) 270-279.

[30] R. Xu, D. Jiang, Y. Zhou, X. Lu, T. Zhang, F. Wang, Influence of 2,6-dihydroxybenzoic acid on the corrosion behavior and discharge performance of AZ31 Mg alloy, Vacuum, 200 (2022) 111031.

[31] B. Vaghefinazari, D. Snihirova, C. Wang, L. Wang, M. Deng, D. Höche, S.V. Lamaka, M.L. Zheludkevich, Exploring the effect of sodium salt of Ethylenediaminetetraacetic acid as an electrolyte additive on electrochemical behavior of a commercially pure Mg in primary Mg-air batteries, Journal of Power Sources, 527 (2022) 231176.

[32] Y. Zhou, S. Zanna, A. Seyeux, L. Wang, P. Marcus, J. Światowska, Influence of sodium 5-sulfosalicylate as a corrosion inhibitor in NaCl electrolyte on enhanced performances of Mg-air batteries, Electrochimica Acta, 435 (2022) 141360.

[33] Z. Song, J. Wang, Y. Song, Z. Chen, H. Zhang, Z. Wu, X. Han, W. Hu, In Situ Interfacial Passivation in Aqueous Electrolyte for Mg-Air Batteries with High Anode Utilization and Specific Capacity, ChemSusChem, 16 (2023).

[34] N. Ling, H. Fan, S. Song, J. Zhang, L. Wang, Enhancement of the discharge behavior for Mg-air battery by adjusting the chelate ability of ionic liquid electrolyte additives, Journal of Energy Storage, 72 (2023) 108709.

[35] S.V. Lamaka, B. Vaghefinazari, D. Mei, R.P. Petrauskas, D. Höche, M.L. Zheludkevich, Comprehensive screening of Mg corrosion inhibitors, Corrosion Science, 128 (2017) 224-240.

[36] Y. Song, D. Shan, E.-H. Han, Pitting corrosion of a Rare Earth Mg alloy GW93, Journal of Materials Science & Technology, 33 (2017) 954-960.

[37] Y.-Q. Zhou, Y. Zhou, J.-T. Li, S. Zanna, A. Seyeux, P. Marcus, J. Światowska, Probing Mg anode interfacial and corrosion properties using an organic /inorganic hybrid electrolyte, Applied Surface Science, 614 (2023) 156070.

[38] D. Kurchavov, U. Rustambek, A. Ottochian, G. Lefèvre, A. Seyeux, I. Ciofini, P. Marcus, V. Lair, P. Volovitch, Synergistic effect of ionic liquid (IL) cation and anion inhibits negative difference effect on Mg in water - IL mixtures, Corrosion Science, 209 (2022) 110723.

[39] Y. Zhou, X. Lu, L. Yang, D. Tie, T. Zhang, F. Wang, Regulating discharge performance of Mg anode in primary Mg-air battery by complexing agents, Electrochimica Acta, 370 (2021).

[40] Y. Zhou, X. Lu, T. Würger, D. Höche, M.L. Zheludkevich, F. Wang, New insights into the inhibition mechanism of carboxylate species on magnesium surface, Corrosion Science, 232 (2024) 112009.

[41] Y. Li, X. Lu, K. Wu, L. Yang, T. Zhang, F. Wang, Exploration the inhibition mechanism of sodium dodecyl sulfate on Mg alloy, Corrosion Science, 168 (2020).

[42] Y. Qiu, X. Tu, X. Lu, J. Yang, A novel insight into synergistic corrosion inhibition of fluoride and DL-malate as a green hybrid inhibitor for magnesium alloy, Corrosion Science, 199 (2022) 110177.

[43] L. Wang, D. Snihirova, M.D. Havigh, M. Deng, S.V. Lamaka, H. Terryn, M.L. Zheludkevich, Non-stationarity in electrochemical impedance measurement of Mg-

based materials in aqueous media, Electrochimica Acta, 468 (2023) 143140.

[44] J.-B. Jorcin, M.E. Orazem, N. Pébère, B. Tribollet, CPE analysis by local electrochemical impedance spectroscopy, Electrochimica Acta, 51 (2006) 1473-1479.

[45] B. Díaz, E. Härkönen, J. Światowska, V. Maurice, A. Seyeux, P. Marcus, M. Ritala, Low-temperature atomic layer deposition of Al2O3 thin coatings for corrosion protection of steel: Surface and electrochemical analysis, Corrosion Science, 53 (2011) 2168-2175.

[46] G.J. Brug, A.L.G.v.d. Eeden, M. Sluyters-Rehbach, J.H. Sluyters, The analysis of electrode impedances complicated by the presence of a constant phase element, Journal of Electroanalytical Chemistry and Interfacial Electrochemistry, 176 (1984) 275-295.

[47] M. Shadi, S. Jolanta, M. Vincent, S. Antoine, H.K. Lorena, H. Emma, R. Mikko, M. Philippe, Electrochemical and Surface Analysis of the Corrosion Protection of Copper by Nanometer Thick Alumina Coatings Prepared by Atomic Layer Deposition, Journal of The Electrochemical Society, 162(8) (2015) C377-C384.

[48] B. Hirschorn, M.E. Orazem, B. Tribollet, V. Vivier, I. Frateur, M. Musiani, Determination of effective capacitance and film thickness from constant-phase-element parameters, Electrochimica Acta, 55 (2010) 6218-6227.

[49] M. Benoit, C. Bataillon, B. Gwinner, F. Miserque, M.E. Orazem, C.M. Sánchez-Sánchez, B. Tribollet, V. Vivier, Comparison of different methods for measuring the passive film thickness on metals, Electrochimica Acta, 201 (2016) 340-347.

[50] I. Yarita, S. Sato, Y. Omura, Proposal of Physics-Based Equivalent Circuit of Pseudo-MOS Capacitor Structure for Impedance Spectroscopy, IEEE Journal of the Electron Devices Society, 4 (2016) 169-173.

[51] T.T.M. Tran, B. Tribollet, E.M.M. Sutter, New insights into the cathodic dissolution of aluminium using electrochemical methods, Electrochimica Acta, 216 (2016) 58-67.

[52] G. Baril, G. Galicia, C. Deslouis, N. Pébère, B. Tribollet, V. Vivier, An Impedance Investigation of the Mechanism of Pure Magnesium Corrosion in Sodium Sulfate

Solutions, Journal of The Electrochemical Society, 154 (2007) C108-C113.
[53] L. Wang, D. Snihirova, M. Deng, B. Vaghefinazari, W. Xu, D. Höche, S.V. Lamaka, M.L. Zheludkevich, Sustainable aqueous metal-air batteries: An insight into electrolyte system, Energy Storage Materials, 52 (2022) 573-597.
[54] Y. Tao, L. Han, Y. Han, Z. Liu, A combined experimental and theoretical analysis on molecular structure and vibrational spectra of 2,4-dihydroxybenzoic acid, Spectrochim Acta A Mol Biomol Spectrosc, 137 (2015) 1078-1085.
[55] K. Govindarasu, E. Kavitha, Vibrational spectra, molecular structure, NBO, UV, NMR, first order hyperpolarizability, analysis of 4-Methoxy-4'-Nitrobiphenyl by density fuctional theory, Spectrochimica Acta Part A: Molecular and Biomolecular Spectrosco, 122 (2014) 130-141.
[56] M.E. Wekre, B. Holmelid, J. Underhaug, B. Pedersen, G. Kopplin, M. Jordheim, Characterization of high value products in the side-stream of Laminaria hyperborea alginate production - Targeting the phenolic content, Algal Research, 72 (2023) 103109.
[57] M. Li, A. Seyeux, F. Wiame, P. Marcus, J. Światowska, Localized corrosion induced surface modifications of Al-Cu-Li alloy studied by ToF-SIMS 3D imaging, npj Materials Degradation, 5 (2021).
[58] S. Thomas, N.V. Medhekar, G.S. Frankel, N. Birbilis, Corrosion mechanism and hydrogen evolution on Mg, Current Opinion in Solid State and Materials Science, 19 (2015) 85-94.
[59] A. Atrens, Z. Shi, S.U. Mehreen, S. Johnston, G.-L. Song, X. Chen, F. Pan, Review of Mg alloy corrosion rates, Journal of Magnesium and Alloys, 8 (2020) 989-998.
[60] S.V. Lamaka, O.V. Karavai, A.C. Bastos, M.L. Zheludkevich, M.G.S. Ferreira, Monitoring local spatial distribution of Mg2+, pH and ionic currents, Electrochemistry Communications, 10 (2008) 259-262.